Simultaneous Aircraft Design & Trajectory Optimisation for Cost Effective Climate Impact Mitigation

A Cost-Climate Trade-off Study

AE5222: MSc FPP Thesis

Nicholas Lambrecht

Delft University of Technology

TU Delft

Simultaneous Aircraft Design & Trajectory Optimisation for Cost Effective Climate Impact Mitigation

A Cost-Climate Trade-off Study

by

Nicholas Lambrecht

Student Name	Student Number
Nicholas Lambrecht	5737524

Responsible Supervisor:	Dr. C. Varriale
Daily Supervisor:	Dr. P. Proesmans
Project Duration:	March, 2024 - October, 2024
Faculty:	Faculty of Aerospace Engineering, Delft

Cover: Distrail over Noordwijk, The Netherlands. Captured by the author.
Word Count: 20 912

TU Delft

Summary

Aviation has drawn increasing attention as an industry with a heavy climate impact, accounting for upwards of 3.5% of global effective radiative forcing (ERF). Two thirds of this is attributed to non-CO_2 effects. As the climate impacts of aircraft emissions become better understood, different avenues are being explored in aircraft design and operations to minimise their effects. State-of-the-art atmospheric modelling and data analysis have shown that the climate impact of aviation is largely affected by the atmospheric regions in which we fly. By redesigning aircraft to fly lower and slower, the climate impact, measured by global average temperature response (ATR), can be significantly reduced. Proesmans and Vos [1] optimised an aircraft for minimum climate impact, assuming a climb-cruise trajectory at constant Mach number. ATR reductions of 50% were observed for 1.8% increase in operating costs. This thesis aims to build on their research by optimising the flight path in more detail. By allowing 2-dimensional vertical flexibility along the flight path, an aircraft can spend more time at a cost-optimal cruise condition, but avoid climate sensitive regions when necessary.

The ATR_{100} refers to the mean temperature change at the Earth's surface over a 100-year period. Emissions from an aircraft fleet are considered to last an extended period of 65 years, throughout which the impact of carbon dioxide, nitrogen oxides (NO_x), sulphates, water vapour and soot are modelled alongside the radiative forcing effect of contrails. Contrails form depending on the atmospheric conditions and can be avoided with relatively small routing modifications. The effects of NO_x are complex and vary considerably depending on emission altitude and engine operating conditions. Given the freedom of a trajectory optimisation, difficulties arise when trying to minimise NO_x effects, and it was thus removed from the ATR objective.

The practicality of climate impact mitigation is considered through a trade-off between the direct operating costs (DOC) and ATR associated with a typical medium range flight at mid-latitude. Focus is placed on narrowbody aircraft, of which the Airbus A320 and Boeing 737 are most common. This guides the study aim: *to evaluate the influence of simultaneous aircraft design and trajectory optimisation on the trade-off between the DOC and ATR of a medium range flight*. The flight paths considered do not include landing and take-off operations (LTO), as these are highly restricted near airports. It is not expected that modifications to LTO flight paths would significantly affect the overall climate response. Furthermore, fleet allocation and more complex 3D or 4D trajectory optimisation are not considered.

Optimal control is used to determine the state and control trajectories which minimise the DOC-ATR objective. It is applied in a monolithic multidisciplinary design optimisation (MDO), allowing both the continuous trajectory and static aircraft design variables to be optimised. The trajectory is transcribed using Legendre-Gauss Radau (LGR) Pseudospectral collocation. The minimisation objective is a variably weighted combination of ATR and DOC. A narrowbody aircraft closely matching an Airbus A320-200, with a DOC-optimal trajectory is taken as the baseline case. Constraints are included on the system parameters to ensure a consistent aircraft design, while state and control bounds keep the aircraft within its flight envelope. Path constraints maintain operational boundaries on the trajectory. The Dymos python library, based on OpenMDAO, offered a suitable platform to build and run the trajectory-aircraft optimisation.

Results show that the ATR associated with a standard narrowbody aircraft covering a 4000km flight can be cost-effectively reduced through vertical plane trajectory optimisation, allowing the aircraft to avoid only isolated regions in which contrails persist instead of modifying the complete cruise path. The significance of contrail avoidance is highlighted by a combined ATR-DOC objective; Even with very high DOC priority, given by a cost weighting of 0.98 (and climate weighting of 0.02), contrail persistence is avoided at the expense of fuel. This indicates that the cost-compromise of avoiding contrail regions is highly worthwhile in the cases studied here.

Simultaneous optimisation of the aircraft alongside the trajectory further improves the ATR and DOC when compared with the cost-optimal baseline. An attractive compromise is shown with a cost weighting of 0.85, where ATR is reduced by 56% and the change in cost is negligible (-0.21%). Flight time for this case increases by 3.5% or just over 10 minutes. The optimal aircraft has a reduced sweep of 14.4 degrees and increased aspect ratio of 11.4.

Preface

Deciding what to be, do or contribute to the world is never straightforward. *Okay, don't get ahead of yourself, this is 'just' a thesis*. Still, I can't deny this is what was going through my mind while trying to pick a topic. After all, it would be eight months of focus which I did not want to spend on something I was not truly passionate about. It also just might impact what I end up working on a few years down the line.

My broad topic idea was 'something to do with aircraft design'. Not very descriptive. I am also passionate about environmental awareness, which is a huge challenge in aviation. Maybe I could target that in some way. Lots of research has been popping up about how to reduce the climate impacts of aviation, but an equal amount about how difficult it is to decarbonise. A third thought was along the lines of work I had done in the past during my final undergraduate project. What if I could take flight path optimisation a little further. Was there *any* way of combining all these topics into one project and still keep it within a year's work?

Now, I dare say that each of them became an integral part of this thesis, and undeniably what kept me motivated throughout. Having said that, what I am most proud of from this work is not the results, nor the fact that it combines three independently complex topics which I could not decide between. It is that I can explain to anyone what my study has been about. I can't count how many times in the last year I have pointed to the sky to explain how bad these white lines (of what is essentially cloud) are for the planet. It doesn't require an engineering degree to understand that a fluffy blanket keeps one warm. I then have the opportunity to explain what they are and that we *can* do something about it. And that 'something' doesn't have to be to simply stop flying.

Of course, not flying would be the most effective option to prevent climate impacts, but that is just not going to happen in the connected world in which we live. If it weren't for air travel, it would take me two weeks just to travel from my home in Cape Town to The Netherlands by ship! To me it seems more sensible to spend that time studying the climate impacts of aviation, and maybe contribute just a tiny bit to our understanding of how to reduce it.

This all makes the experience of thesis-writing sound quite peachy, and there were parts which were: getting my first optimised trajectories, seeing results of how much climate impact could be reduced, and really beginning to understand what I was seeing in the sky (with particular reference to the distrail on the front cover, which I captured while cycling past Noordwijk). However, in between the highs there were weeks which felt as if absolutely no progress was made and I wondered if everything would fall apart. The only thing helping me through those weeks were the people around me.

Special thanks must go to my supervisors, Carmine and Pieter-Jan, who were always available for some banter before the serious meetings began. They would always point out what progress I *had* made when I couldn't see it, and encourage me that 'no one has ever done quite what you are doing - of course it will be difficult'. I must thank my friends, and officemates, with whom I could share the struggles of solitary research and seemingly endless coding problems. Also for their ridiculous humour that would make lunch breaks a daily highlight. Finally, I must thank my family back home, who would always be ready for a chat, whether I was in a phase of excitement at new results or the doldrums in between. I could not have done any of this without them.

Nicholas Lambrecht
Delft, October 2024

Contents

Nomenclature

Table 1: Definition of Abbreviations.

Abbreviation	Definition	Context
AiC	Aviation-induced Cloudiness	Climate Forcer
ATO	Aircraft Trajectory Optimisation	Methodology
ATR	Average Temperature Response	Climate Metric & Objective
BPR	Bypass Ratio	Engine Design Parameter
BWB	Blended Wing Body	Aircraft Configuration
CCF	Climate Change Function	Climate Modelling
CPR	Contrail Persistence Region	Climate Modelling
CiC	Contrail-Induced Cirrus	Climate Forcer
CRA	Climate-Restricted Airspaces	Operational Measure
DOC	Direct Operating Cost	Market Factor & Objective
EMAC	ECHAM5/MESSY Atmospheric Chemistry Model	Climate Modelling
(A)GTP	(Absolute) Global Temperature Potential	Climate Metric
GWP	Global Warming Potential	Climate Metric
ICAO	International Civil Aviation Organisation	Operations Regulations
ISA	International Standard Atmosphere	Climate Modelling
ISSR	Ice-Supersaturated Region	Climate Modelling
MDF	Multidisciplinary Feasible	Methodology
MDO	Multidisciplinary Design Optimisation	Methodology
MTOM	Maximum Take-Off Weight	Aircraft Parameter
OCP	Optimal Control Problem	Methodology
OEM	Original Equipment Manufacturer	Stakeholder
OPR	Overall Pressure Ratio	Design Parameter
(E)RF	(Effective) Radiative Forcing	Climate Metric
RPK	Revenue-Passenger-Kilometer	Market Metric
SAC	Schmidt-Appleman Criterion	Climate Modelling
SAND	Simultaneous Analysis and Design	Methodology
SBW	Strut-Braced Wing	Aircraft Configuration
SFC	Specific Fuel Consumption	Performance Metric
SLCP	Short-Lived Climate Pollutants	Climate Modelling
TET	Turbine Entry Temperature	Engine Design Parameter

Table 2: Definition of Symbols.

Symbol	Definition	Unit
$\boldsymbol{a}$	Speed of Sound	m/s
A	Aspect Ratio	-
$\boldsymbol{D}$	Aerodynamic Drag Force	N
$\dot{\boldsymbol{E}}$	Emission Rate	kg/s
$\boldsymbol{F_T}$	Thrust Force	N
$\boldsymbol{g}$	Optimisation Constraints	normalised vector [1]
$\boldsymbol{h}$	Altitude	m
H	ATR Time Horizon	years

[1] Individual components normalised by their reference values given in table 3.2.

Table 2: Definition of Symbols.

Symbol	Definition	Unit
RH	Relative Humidity	-
SH	Specific Humidity	kg/kg
$\boldsymbol{L}$	Aerodynamic Lift Force	N
$\boldsymbol{m}$	Aircraft Mass	kg
$\boldsymbol{M}$	Flight Mach Number	-
$\boldsymbol{p}$	Atmospheric Pressure	Pa
$\boldsymbol{r}$	Range	m
$\boldsymbol{t}$	Time	s
$\boldsymbol{T}$	Atmospheric Temperature	K
$\boldsymbol{T_{t4}}$	Turbine Entry Temperature	K
$\boldsymbol{u}$	Control Vector	normalised vector [1]
$\boldsymbol{v}$	Airspeed	m/s
$\boldsymbol{W/S}$	Wing Loading	N/m^2
$\boldsymbol{x}_p$	Design Parameter Vector	normalised vector [1]
$\boldsymbol{z}$	Optimisation Parameter Vector	normalised vector [1]
$\boldsymbol{\alpha}$	Angle of Attack	degrees
δ_T	Throttle	-
$\boldsymbol{\gamma}$	Flight Path Angle	degrees
$\boldsymbol{\lambda}$	Adjoint Multipliers	-
$\mathcal{L}$	Lagrange/Running Cost Function	-
$\boldsymbol{\rho}$	Atmospheric Air Density	kg/m^3
$\boldsymbol{\xi}$	State Vector	normalised vector [1]
$\boldsymbol{\Phi}$	Mayer/End Cost Function	-

Table 3: Definition of Subscripts.

Subscripts	Definitions
0	Initial Condition
j	Intermediate Condition
f	Final Condition
EoO	End of Operation
LB	Lower Bound
UB	Upper Bound

Table 4: Definition of Chemical Formulae.

Formula	Name
CO_2	Carbon Dioxide
H_2O	Water Vapour
NO_x	Nitrogen Oxides (NO, NO_2)
NO_x-CH_4	NO_x-Induced Methane
NO_x-O_{3L}	NO_x-Induced Long-Term Ozone
NO_x-O_{3S}	NO_x-Induced Short-Term Ozone
SO_4	Sulphate

1 Introduction

1.1. Background

Aircraft fuel efficiency has improved steadily over the last decades, with fuel burn per tonne-km decreasing by 41% between 1970 and 2019 [2]. However, in recent years the annual rate of improvement has gradually decreased, while the aviation industry has faced increasing pressure to decarbonise. Studies have shown that 3.5% of anthropogenic effective radiative forcing (ERF), or 4.9% including contrail-induced cirrus (CiC), is attributed to aviation [3, 4, 5]. This is predicted to continue to increase consistently by 4-5% annually [6]. While many industries consider only carbon dioxide emissions as climate impacting, two thirds of the net ERF caused by aviation is due to non-CO_2 emissions [3]. Focus should therefore be placed on reducing all climate impacting emissions species, rather than on fuel burn and CO_2 emissions. Many avenues are being approached to this end, including novel aircraft concepts, progressive engine technologies, alternative fuels and operational changes.

1.2. Climate Impact Measurement

Climate impact can be defined in several ways and depends on the disturbance or measure of interest. A proper definition must therefore be chosen. Environmental impact can be classed as the effect of either aircraft noise or gaseous emissions. This study will focus on gaseous emissions, including carbon dioxide (CO_2), nitrogen oxides (NO_x), sulphates (SO_4) and unburned hydrocarbons (UHCs) or soot. Furthermore, water vapour (H_2O), contrails and contrail-induced cirrus (CiC) have considerable longer-term impacts on the environment [7].

Unlike CO_2 emissions - the traditional climate metric for non-aviation industries - other emissions from aviation have a strong regional impact. In particular, contrails form only in regions with the right humidity for condensation of exhaust gases, but not so high that clouds already exist. Furthermore, the temperature must be below -38°C to promote freezing of condensed droplets. Finally, contrails will only persist for long periods in ice-supersaturated regions (ISSRs) of the atmosphere [8], meaning that the frozen particles will not dissolve. ISSRs typically extend around 500m vertically and 100km horizontally [9]. These conditions often occur in the upper troposphere or lower stratosphere - a typical cruise altitude for commercial aircraft. However, this *altitude* at which contrails most commonly form varies with *latitude* due to temperature and humidity differences between the equator and the poles. In low to mid latitudes, contrails can be avoided by reducing cruise altitude. At high latitudes, however, contrails might be better minimised by flying higher (up to around 14km) [10].

Widely-used measures of climate impact are global warming potential (GWP) and average temperature response (ATR). Megill [11] concluded that the ATR "is the most appropriate climate metric for aviation climate policy", although the time period over which it is taken can be subjective. ATR is a metric developed specifically for evaluating the climate impact of aviation and estimates the near-surface temperature change over a specified time period. Rather than considering a once-off pulse emission, ATR is unique in that it considers a sustained lifetime emission and averages the surface temperature change over a defined period, typically 20, 50 or 100 years [11].

1.3. Climate Impact Mitigation in Aviation

1.3.1. Engine Technology

Engine technology improvements such as geared turbofans and increased overall pressure ratio (OPR) and turbine entry temperature (T_{t4}) have enabled higher bypass ratios (BPR) and improved efficiency. The objective has mostly been to reduce fuel consumption and operating cost. However, a side effect of higher combustion temperatures is increased thermal NO_x emission [12], a gas with indirect global warming potential (GWP) of more than 30 times that of CO_2 for a 20 year horizon [13]. NO_x has the effect at high altitudes of enhancing production of ozone in the short term and depleting methane and ozone in the long term [1]. Higher BPR engines also have the side effect that cooler air is expelled, increasing the chance of persistent contrail formation as the exhaust mixes with surrounding air. Contrails contribute significantly to the climate impact of aviation through radiative forcing [3].

1.3.2. Alternative Fuels

Alternative fuels such as sustainable aviation fuel (SAF) and hydrogen offer possibilities of reducing life cycle emissions. In the best case, SAF could become carbon neutral and offer reductions in particulate emissions, particularly sulphur-oxides (SO_x) and soot, of 50-97% [14]. Because of this, SAF would have less impact on local air quality and may also reduce contrail formation. However, ethical concerns surround the issue of SAF production, such as the diversion of food resources and pressure to free up more natural spaces for agriculture. Scaling up production will therefore be a challenge.

Hydrogen fuel could ideally become carbon-free. It could be used either in combustion or fuel cell architecture, both of which are being developed in the Airbus ZEROe project. But numerous hurdles remain, such as the impact of hydrogen leaks, increased formation of contrails due to the high water vapour content of the exhaust, and NO_x production due to the very high combustion temperatures. Large-scale production of green hydrogen will also be a challenge.

1.3.3. Novel Aircraft Configurations

Grewe et al. [15] recognise the potential of novel aircraft configurations, particularly strut-braced wing (SBW) aircraft with open rotor engines, which promise increased fuel efficiency and reduced NO_x emissions. A lower cruise altitude than a comparable narrowbody aircraft also contributes to reduced climate impact. Particulate emissions could be reduced by using leaner combustion engines appropriate for SBW aircraft, which would change the properties of contrails and further limit climate impact. Blended-wing-body (BWB) aircraft may also offer increased seating density for the equivalent whetted aircraft surface area, leading to improvement of fuel consumption per revenue-passenger-kilometre (RPK). Airbus claims that BWB aircraft could improve fuel efficiency by 20% over current single-aisle planes [16], and the Flying-V concept has shown the potential to improve lift-to-drag by 21% over an equivalent twin-aisle aircraft [17]. JetZero, which announced FAA clearance of their BWB demonstrator in March 2024, claims that their design should reduce fuel consumption by 50% [18].

1.3.4. Aircraft Optimisation

Recently, studies have shifted from optimising aircraft for improved direct operating cost (DOC) or fuel consumption [19, 20, 21], to focus on more generalised climate impact measures [1, 15]. However, the flight profile is often assumed highly simplified or disconnected from the aircraft optimisation. In their study optimising aircraft design to minimise climate impact, Proesmans and Vos [1] assumed a continuous cruise-climb and constant Mach number. They note that optimisation of the flight profile would provide a valuable extension to their work, particularly if done simultaneously with an aircraft optimisation. That is the goal of this study.

1.3.5. Trajectory Optimisation

Methods to independently optimise aircraft trajectories based on fixed aircraft designs have been well studied. In a comparative study between real flight data and optimal trajectory flights, Boucher et al. [22] showed that fuel consumption can be reduced by 1-10%, depending on the required route. With more focus on climate impact, Lührs et al. [9] used optimal control theory to develop a cost-benefit assessment of climate optimised trajectories. Their work assessed nine standard North Atlantic routes, where ATR reductions of approximately 15% and 18-20% are seen for 2D and 3D optimised trajectories respectively, while limiting operating cost to increase by only 2%. However, they report

that to achieve minimum climate impact without a multi-objective approach would raise operating cost impractically. Other flight path developments have considered the effect of atmospheric winds [23] or proposed methods of in-flight profile adjustment based on changing weather conditions [24]. However, these studies still view the trajectory independently from aircraft design.

Due to the highly regional nature of ISSRs and contrail formation, trajectory optimisation could be used to reroute aircraft to areas with far lower climate impact. It is therefore important to define and avoid climate sensitive areas which are more prone to persistent contrail and cirrus formation. However, enforcing a rule on avoidance of these areas will be an operational challenge. Niklaß et al. [25] proposed that climate restricted airspaces (CRAs) could be implemented with a form of penalty to aircraft passing through these regions. Simorgh et al. [26] quantified climate sensitive regions using "algorithmic climate change functions." They recognise that airspace structure is a practical challenge that must be addressed by trajectory optimisation, and thus they constrain the problem appropriately.

1.3.6. Simultaneous Aircraft Design and Trajectory Optimisation

Allison and Herber [27] recognised the advantages of integrating the design of a physical system and its control, since they can be strongly coupled in a dynamic system. They discuss MDO formulations for such dynamic systems in the general case. Kaneko and Martins [28] applied this to aircraft design and flight profile optimisation. They showed that a fuel burn improvement of 4.23% can be achieved by optimising an aircraft wing design and trajectory simultaneously, compared to sequential optimisation of the two disciplines. They compare different MDO architectures and coupling strategies to provide valuable insights into the computational efficiency of trajectory optimisation in aircraft design. Hwang, Jasa and Martins [29] perform a multidisciplinary optimisation of aircraft design, flight profile and aircraft allocation, improving airline profits by 2%.

1.4. Research Objective

The methods presented above have been well studied by research institutions, airlines and original equipment manufacturers (OEMs). However, with non-CO_2 emissions complicating the challenge of climate impact mitigation in aviation, studies on optimisation in this area are somewhat lacking. Some studies [28, 29] combine trajectory optimisation and aircraft design, but with a cost objective rather than one of climate impact. Research by Proesmans and Vos [1] focuses on aircraft design for minimum climate impact, but the effect of an optimal trajectory is not considered. This presents a gap in research, where the topics of aircraft design, trajectory optimisation and climate impact could be combined. Building on the work of Proesmans and Vos [1], the research objective is:

To contribute to the conversation on how we might limit anthropogenic climate change in a cost-effective manner through simultaneous aircraft design and trajectory optimisation.

Three main pillars of research are brought together:

- Trajectory Optimisation
- Aircraft MDO
- Climate Impact

These topics were used as the basis of the literature search described in Section 2.1, and they prompt the research question in Section 1.5. To ensure economic feasibility, a major goal of this research is to determine the relationship between direct operating costs (DOC) and the climate impact measured in average temperature response (ATR). Thus, the research objective considers the COC-ATR trade-off of a medium-range flight to demonstrate the effect of simultaneous aircraft design and trajectory optimisation.

Outside the scope of this work is to consider fleet allocation within an airport network. This is the selection of certain aircraft types and their fleet quantities depending on the demand in a given network. Instead, a given typical flight range and payload will be used to develop the trajectory optimisation algorithm. Instead, a fixed fleet definition considers a given number of flights per year, which varies from the date of introduction of the first aircraft to the retirement of the last. Comparing routes of different range, payload and atmospheric condition will add some generality to the study.

1.5. Research Question

The following research question is posed:

What is the influence of simultaneous aircraft and trajectory optimisation on the trade-off between the average temperature response and direct operating costs associated with medium-range flights?

This question encompasses the major topics of interest, while placing focus on trajectory optimisation as the primary technical challenge of this work. A variable cost weighting is used to optimise the system for a combined DOC and ATR weighted objective, where priority can be shifted between the two. To answer the research question, the following scenarios are compared to evaluate the effect of simultaneous optimisation.

- Cost-optimal trajectory with baseline aircraft (baseline case).
- Optimised trajectory with baseline aircraft for varied cost weightings.
- Simultaneously optimised aircraft and trajectory for varied cost weightings.

The study is based on narrowbody aircraft optimisation, taking baseline parameters from the Airbus A320-200 as one of the most commonly used aircraft for medium range flights [30]. A standard aircraft optimised for direct operating cost therefore provides the experimental baseline against which optimised designs and trajectories can be compared. In practice, aircraft are used over a wide variety of flight distances, meaning that they often fly out of their optimal design case. It is therefore of interest to compare results for different range and payload combinations.

Of the three pillars described in the aim (Section 1.4), two have been combined by several studies with favourable results. Trajectory optimisation for minimum climate impact is covered by Hammad et al. [7], Lührs et al. [9] and Sridhar, Ng and Chen [23]. Aircraft design and trajectory optimisation have been combined by Kaneko and Martins [28] and Yan, Jansen and Perez [31]. Finally, a focus on aircraft design to minimise climate effects has been studied by Proesmans and Vos [1] and Antoine and Kroo [19]. It is therefore expected that introducing optimal trajectory into an aircraft MDO will improve the climate optimality by a significant margin.

1.6. Report Structure

In the following pages, Chapter 2 covers state of the art theory relevant to this work, beginning with a short description in Section 2.1 of how the literature review was conducted. Section 2.2 discusses some background to optimal control methods and the most widely-used methods of transcribing and solving the problem. Section 2.3 provides a brief description of formulations and trade-offs of different MDO architectures. Climate modelling is discussed in Section 2.4.

Chapter 3 presents the methodology used to build the modules defining and analysing the aircraft and trajectory. It is divided into sections on the overall problem structure (Sec. 3.1), aircraft parametrisation (Sec. 3.2) and trajectory optimisation (Sec. 3.3). The climate model is described in detail in Section 3.4. Experimental cases defined by range, payload and atmospheric conditions are presented in Section 3.5.

Chapter 4 presents the results, first for the baseline aircraft (Sec. 4.1), then for cases with simultaneous aircraft optimisation (Sec. 4.2), both based on a medium range flight. The two scenarios are brought together and compared in Section 4.3. A sensitivity analysis examining each of the aircraft design variables is presented in Section 4.4. The effects of varied atmospheric humidity are explored in Section 4.5, and an alternative short range scenario is tested in Section 4.6. Conclusions are drawn in Section 5. Recommendations and suggested future research are discussed in Chapter 6.

2

State of the Art

2.1. Literature Search

Based on the discussion presented in the introduction, a research gap was identified in the field combining aircraft design, trajectory optimisation and climate impact. Table 2.1 presents the terms used in the literature search in Scopus. Each of the main topics are covered, and related terms used in the search are given in the table body.

Table 2.1: Literature Search Terms

Aircraft	Trajectory	Optimal Control Theory	Climate Impact
aircraft	trajector*	optimal control	climate
airliner	flight path	optimiz*	pollut*
fixed wing	flight profile	optimis*	emission*

The initial search generated 654 results, of which 284 were from 2021 or later. This indicated that the area of research is active, despite classical optimal control theory dating back to the 17th and 18th centuries when the *calculus of variations* was developed [32]. Limiting the search results to articles published since 2016, and filtering out papers relating to social factors, noise, aerodynamics, traffic management, UAVs, defence aircraft and ground-based transport reduced the number of results to 351. However, a large portion of the remaining results were still not relevant to the aim of this project. Many were related to operational improvements such as reducing operating costs or flight time, or better management of landing and takeoff operations for reduced traffic congestion or improved air quality. Figure 2.1 shows the number of results retrieved from each of the top 5 subject areas. The division indicates that most topics are relevant to engineering and climate science. Topics in the areas of computer science and mathematics might also be relevant to the Optimal Control Problem.

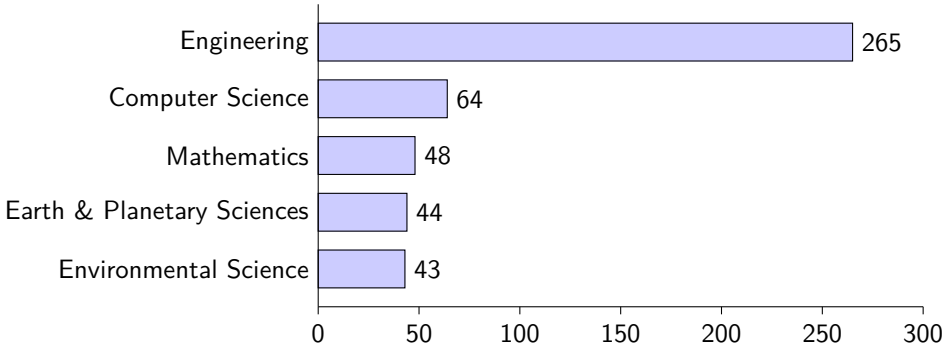

Figure 2.1: Paper Division by Subject Area

From inspection of titles and abstracts, roughly 1 in 10 of the remaining articles were directly relevant

to this study, relating either to aircraft trajectory optimisation theory or its application in a climate impact study. Many of these influenced the progression of this project and appear throughout the text.

2.2. Trajectory Optimisation

2.2.1. Background to Optimal Trajectories

In atmospheric flight, trajectory optimisation for minimum climate impact is interesting and complex because of the variability of atmospheric properties leading to isolated regions of climate sensitivity. Aerosol presence, water vapour content and temperature are of particular interest in considering contrail formation and persistence. If conditions are right, contrails will condense, freeze and persist for many hours. On the other hand, time and fuel related costs are important to airlines in their mission to generate profit. For customers, flight duration and departure/arrival times impact their journey comfort and convenience. Thus, in forming the optimisation objective, trajectories will need to consider the climate, time related costs and fuel usage.

Figure 2.2 illustrates how cost-optimal and climate optimal trajectories might differ. Typically, a constant climb-cruise flight leads to minimum cost, as high-altitude flight in low density air is time and fuel efficient. This is often in contradiction with a climate optimal path, which favours lower and slower flight. The figure demonstrates how ice-supersaturated regions (ISSRs) could be avoided to minimise climate impact. Once water vapour from an aircraft engine exhaust condenses and freezes below -38°C, it can persist for many hours in an ISSR - an area of the atmosphere with relative humidity with respect to ice of greater than 100%, meaning that ice particles do not sublimate.

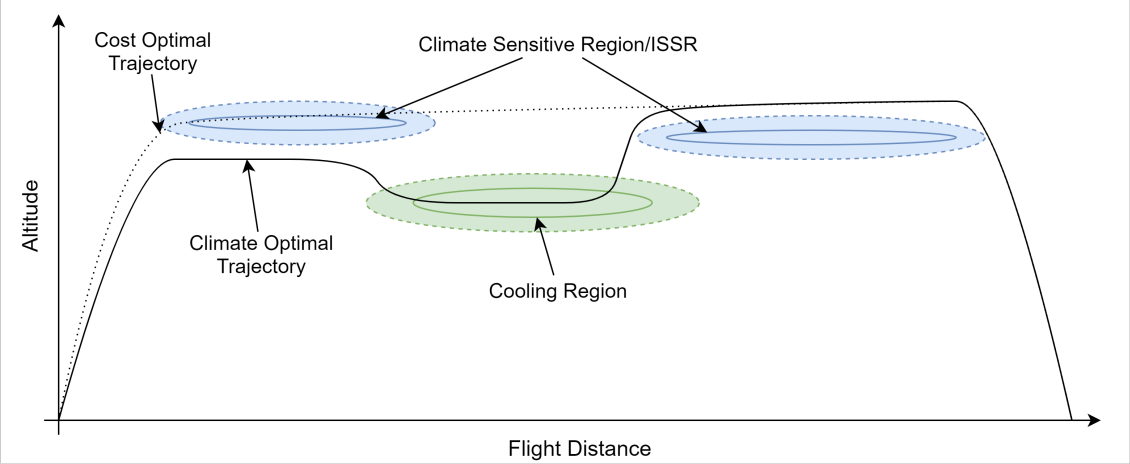

Figure 2.2: Example of a 2D Climate Optimised Trajectory

From an operational viewpoint, flight paths are restricted by airspaces and flight levels to ensure safe separation of aircraft. Geographic features might also play a practical role in aircraft routing. These are hard constraints which must be avoided for safety reasons, and should be treated as *no-go* regions of the trajectory space.

Considering the above, it is necessary to explore the nature of trajectory development relevant to this study. A trajectory space can include up to 4 dimensions. Generally, a 2D trajectory includes either vertical or horizontal freedom in the flight path. 3D optimisations allow more freedom, enabling advanced manoeuvres for consideration of airspaces and atmospheric regions. If a time component is included in the trajectory, it is referred to as 4D optimisation [33, 34]. This can be useful when flight duration is of importance, but it also allows consideration of changing atmospheric conditions [9]. Lim, Gardi and Sabatini [35] used a 4D optimisation to limit the formation of contrails by avoiding sensitive atmospheric regions and considering the optimal time of day for which minimum radiative forcing results.

Ultimately, a 4D optimised trajectory is likely to yield highly favourable results in minimising climate impact while limiting additional cost or flight time. However, the complexity of the climate model and control problem is beyond the scope of this study. Although 3D optimisations have proven more effective than their 2D counterparts (Lührs et al. [9] found a 20-35% further reduction in climate impact

for 3D lateral-vertical optimisation compared to 2D lateral or horizontal optimisation), a large portion of the improvement can be achieved even with a 2D optimal trajectory, and the problem complexity is minimised. However, unlike the study by Lührs et al. [9] in which the 2D optimisation only considered horizontal deviations, a vertical 2D optimisation seems more appropriate for avoidance of ISSRs. It is easily visualised, as illustrated in Figure 2.2. The figure also represents cooling regions, which may occur due to phenomena such as *distrails* (as shown in the cover image). There are a variety of explanations for this phenomenon, one of which relates the wake disturbance of a passing aircraft to freezing of cloud condensation, which then drops to lower altitudes and sublimates. Others suggest that expelled soot increases condensation nuclei and triggers freezing.

2.2.2. The Optimal Control Problem

A trajectory $\boldsymbol{\xi}(t)$ is the evolution of the state of a dynamic system over time. The trajectory is influenced by a control $\boldsymbol{u}(t)$ and parameters $\boldsymbol{x}_p$ which represents the physical system. Parameters are typically fixed in optimal control problems, but in simultaneous design and trajectory optimisations they comprise the aircraft design variables, as they affect the system dynamics [28]. In the general case, there are n states, m controls and q design parameters:

$$\boldsymbol{\xi}(t) \in \mathbb{R}^n; \quad \boldsymbol{u}(t) \in \mathbb{R}^m; \quad \boldsymbol{x}_p \in \mathbb{R}^q \tag{2.1}$$

The optimal control problem, where design parameters $\boldsymbol{x}_p$ are constant, aims to optimise the *performance index* J between the starting and ending times $t \in [t_0, t_f]$, which may be defined as

$$J = \Phi[\boldsymbol{\xi}(t_f), t_f; \boldsymbol{x}_p] + \int_{t_0}^{t_f} \mathcal{L}[\boldsymbol{\xi}(t), \boldsymbol{u}(t), t; \boldsymbol{x}_p] dt \tag{2.2}$$

The *end cost* function Φ (Mayer term) evaluates the optimality of the trajectory at its final state, whereas the *running cost* term $\mathcal{L}$ describes the optimality of the trajectory over its progression and is known as the Lagrange term. When the terminal cost term is included, the problem is referred to as a Bolza objective. In simultaneous aircraft design and trajectory optimisation, the system is subject to *dynamic constraints* (Eqn. 2.3), *path constraints* (Eqn. 2.4), *boundary conditions* (Eqn. 2.5) and *static design constraints* (Eqn. 2.6).

$$\dot{\boldsymbol{\xi}} = \boldsymbol{f}\left(\boldsymbol{\xi}(t), \boldsymbol{u}(t), t; \boldsymbol{x}_p\right) \tag{2.3}$$

$$\boldsymbol{g}_{\text{path}}\left(\boldsymbol{\xi}(t), \boldsymbol{u}(t), t; \boldsymbol{x}_p\right) \leq \boldsymbol{0} \tag{2.4}$$

$$\boldsymbol{g}_{\text{bound}}\left(t_0, t_f, \boldsymbol{\xi}(t_0), \boldsymbol{\xi}(t_f)\right) \leq \boldsymbol{0} \tag{2.5}$$

$$\boldsymbol{g}_{\text{static}}(\boldsymbol{x}_p) \leq \boldsymbol{0} \tag{2.6}$$

Bounds can be present on the state (Eqn. 2.7), control (Eqn. 2.8) and design variables (Eqn. 2.9).

$$\boldsymbol{\xi}_{\text{LB}} \leq \boldsymbol{\xi} \leq \boldsymbol{\xi}_{\text{UB}} \tag{2.7}$$

$$\boldsymbol{u}_{\text{LB}} \leq \boldsymbol{u} \leq \boldsymbol{u}_{\text{UB}} \tag{2.8}$$

$$\boldsymbol{x}_{p,\text{LB}} \leq \boldsymbol{x}_p \leq \boldsymbol{x}_{p,\text{UB}} \tag{2.9}$$

The optimisation problem is typically transformed into a non-linear programming (NLP) problem. The performance index is reformulated as an *augmented performance index* $\overline{\boldsymbol{J}}$ by adjoining the dynamic constraints of Equation 2.3. Note that dependencies of the terms are removed for readability.

$$\overline{\boldsymbol{J}} = \Phi + \int_{t_0}^{t_f} \left[\mathcal{L} + \boldsymbol{\lambda}^T(\boldsymbol{f} - \dot{\boldsymbol{\xi}})\right] dt \tag{2.10}$$

The Hamiltonian is introduced for convenience

$$H[\boldsymbol{\xi}, \boldsymbol{\lambda}, \boldsymbol{u}, t; \boldsymbol{x}_p] = \mathcal{L}[\boldsymbol{\xi}(t), \boldsymbol{u}(t), t; \boldsymbol{x}_p] + \boldsymbol{\lambda}^T \boldsymbol{f}[\boldsymbol{\xi}(t), \boldsymbol{u}(t), t; \boldsymbol{x}_p] \tag{2.11}$$

so that the performance index becomes

$$\overline{\boldsymbol{J}} = \Phi + \int_{t_0}^{t_f} \left[H - \boldsymbol{\lambda}^T \dot{\boldsymbol{\xi}}\right] dt \tag{2.12}$$

2.2.3. Problem Transcription

Transcription is the transformation of a trajectory optimisation problem into a constrained parameter optimisation which can be solved numerically with methods such as non-linear programming (NLP). It entails discretisation of the continuous trajectory into a number of nodes at which states, controls and constraints are evaluated. The NLP problem might take the following form:

$$\min_{z} \boldsymbol{f}(\boldsymbol{z}) \quad \text{subject to:} \quad \boldsymbol{g}(\boldsymbol{z}) \leq \mathbf{0}; \quad \boldsymbol{z}_{\text{low}} \leq \boldsymbol{z} \leq \boldsymbol{z}_{\text{high}} \tag{2.13}$$

where $\boldsymbol{f}$ is the minimisation function and $\boldsymbol{g}$ are the inequality constraints, which can be formulated also as equalities. The discretised parameters $\boldsymbol{z}$ are subject to bounds $\boldsymbol{z}_{low}$ and $\boldsymbol{z}_{high}$.

Transcription reduces the vector functions and differential equations of the optimal control problem (OCP) to a discretised set of real numbers and algebraic expressions which are more easily solved. For any practically complex OCP, a numerical solver is necessary. Methods for transcribing trajectory problems are typically classified as either indirect methods or direct methods [36]. Direct methods are widely documented and most commonly used, although indirect methods have also been used. Hammad et al. [7] also explored the methods of dynamic programming and meta-heuristics (or machine learning). However, they explain that dynamic programming methods experience an exponential increase in state space size and become inefficient in solving ATO problems. Although machine learning might offer new methods of solving ATO problems, such as that demonstrated by Xu et al. [34], the approach is relatively new and fundamentally different to classic optimal control. The following subsections will present some trade-offs between indirect and direct methods, followed by a comparison of discretisation techniques and finally a discussion on mesh refinement.

Direct vs Indirect Methods

Direct and indirect methods differ in how the problem is transcribed. An *indirect method* aims to first compute the optimality conditions of a problem. It then solves the problem using *calculus of variations* by converting it to a two-point boundary value problem, where it is discretised in the numerical solver. *Direct methods* switch this around, first discretising the problem and then optimising its individual segments, ensuring continuity with additional constraints [7]. Rather than relying on calculus of variations, direct methods generate a finite-dimensional parametrisation of linearly independent functions of the form:

$$\boldsymbol{y}(t) \approx \sum_{k=1}^{N} \boldsymbol{a}_k q_k(t) \tag{2.14}$$

where $\boldsymbol{y}(t)$ can be used to parametrise the state, the control or both. The term $\boldsymbol{q}_k(t)$ is a set of known basis functions and $\boldsymbol{a}_k$ is a set of unknown coefficients. Direct methods are typically much easier to solve for complex problems than indirect methods.

Discretisation

Both shooting and collocation methods are commonly used to discretise optimal control problems. Shooting methods use explicit discretisation and system simulation to determine the state evolution under a given initial state and control. The error on the final state (or intermediate states for *multiple shooting*) is used to update the control.

Simple shooting is the most basic indirect method, where an unknown initial condition (state and control) is guessed, the system reaction determined through time-marching simulation and the final state is compared to the desired outcome. It is likened to shooting at a target, observing the error and adjusting the initial release angle and power of the projectile. While this method is easily implemented, it can suffer from ill-conditioning, where a small change in the boundary conditions or control has a large effect on the trajectory, particularly for large time intervals [36]. *Multiple shooting* attempts to overcome numerical difficulties of simple shooting by dividing the time interval into subintervals as illustrated in Figure 2.3. Simple shooting is applied to each subinterval and continuity is ensured by setting the state $\boldsymbol{x}(t_i)$ and adjoint $\boldsymbol{\lambda}(t_i)$ equal at each subinterval interface (collectively referred to as $\boldsymbol{z}(t)$). Thus, the error to minimise at interface i is $\epsilon_i = \boldsymbol{z}(t_i^-) - \boldsymbol{z}(t_i^+)$. Although multiple shooting introduces additional variables at each interface, it performs better than simple shooting because of the far smaller time-integrated intervals.

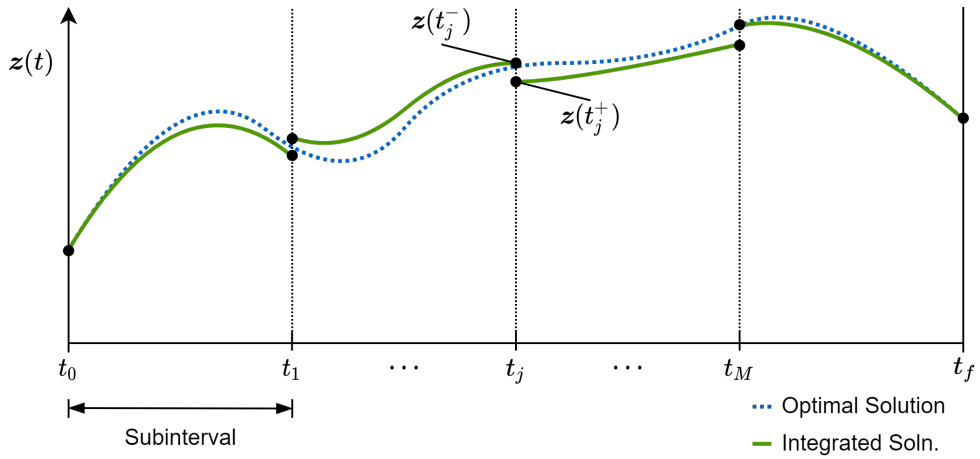

Figure 2.3: Multiple Shooting

Alternatively, *collocation methods* use function approximation and implicit integration to approximate system dynamics based on a discretised state and control. The solution is found over a number of iterations by varying and improving the state and control approximations to match the dynamic system. If only the control is parametrised, the system dynamics (Eqn. 2.3) can be explicitly integrated. The performance index (Eqn. 2.2) is approximated through quadrature [36]. A non-linear optimisation problem arises, in which the unknown coefficients are solved as the optimisation vector $\boldsymbol{z}$.

In ATO problems, direct methods which parametrise both the state and control are considered most suitable [7, 28, 36]. In this case, the optimisation vector $\boldsymbol{z}$ contains the constants for both the state $\boldsymbol{b}_k$ and control $\boldsymbol{c}_k$, which are parametrised as

$$\boldsymbol{\xi}(t) \approx \sum_{k=0}^{N-1} \boldsymbol{b}_k q_k(t); \quad \boldsymbol{u}(t) \approx \sum_{k=0}^{N-1} \boldsymbol{c}_k q_k(t) \tag{2.15}$$

The state can no longer be explicitly integrated, so implicit integration is used. The time interval $t \in [t_0, t_f]$ is divided into $M+1$ subintervals with nodes $t_1, ..., t_M$ as shown in Figure 2.4. A new set of integrals can be defined over the subintervals $[t_i, t_{i+1}]$, resulting in an expression for the state at subsequent nodes:

$$\boldsymbol{\xi}(t_{i+1}) = \boldsymbol{\xi}(t_i) + \int_{t_i}^{t_{i+1}} \boldsymbol{f}[\boldsymbol{\xi}(s), \boldsymbol{u}(s), s; \boldsymbol{x}_p] ds \tag{2.16}$$

The integral can be approximated by quadrature with nodes $\tau_l (l = 1, ..., Q)$, and using the function approximations in Equation 2.15, giving:

$$\int_{t_i}^{t_{i+1}} \boldsymbol{f}[\boldsymbol{\xi}(s), \boldsymbol{u}(s), s; \boldsymbol{x}_p] ds \approx \sum_{l=1}^{Q} \beta_{il} \boldsymbol{f}[\boldsymbol{\xi}(\tau_l), \boldsymbol{u}(\tau_l), \tau_l; \boldsymbol{x}_p] \tag{2.17}$$

Similarly, the performance index integral is approximated using quadrature:

$$\int_{t_i}^{t_{i+1}} \boldsymbol{\mathcal{L}}[\boldsymbol{\xi}(s), \boldsymbol{u}(s), s; \boldsymbol{x}_p] ds \approx \sum_{l=1}^{Q} \beta_{il} \boldsymbol{\mathcal{L}}[\boldsymbol{\xi}(\tau_l), \boldsymbol{u}(\tau_l), \tau_l; \boldsymbol{x}_p] \tag{2.18}$$

Hammad et al. [7] recommend direct collocation methods as well-suited to ATO problems because of how the dynamic equations are enforced with quadrature. Effectively, these are added problem constraints and therefore they prevent inconsistencies which might otherwise result when using shooting methods. Kaneko and Martins [28] use collocation methods in their simultaneous trajectory and aircraft design problem. Rao [36] claims that using state and control parametrisation, and hence implicit collocation methods, are by far the most powerful of those discussed because of how derivatives of the NLP are found. Since collocation methods approximate each segment of a trajectory with linearly independent functions, each of these can be perturbed at every iteration, whereas in shooting methods only vary one value per subinterval at a time [37].

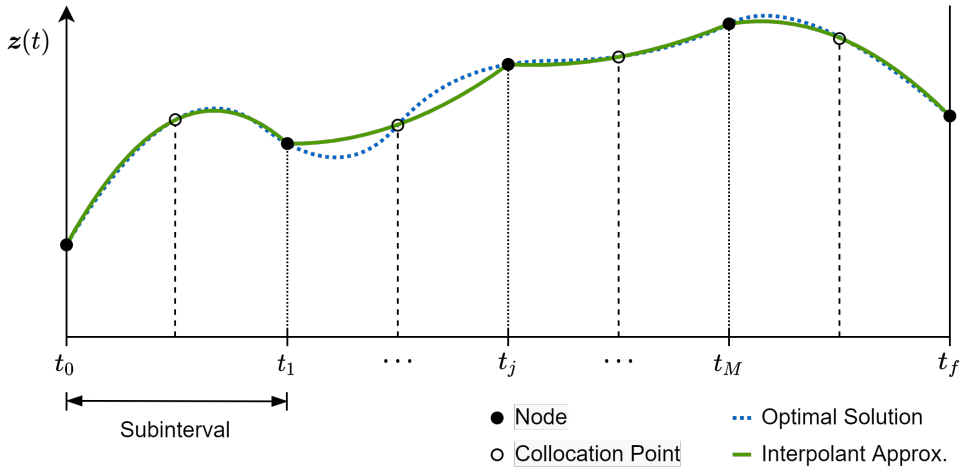

Figure 2.4: Collocation Interval Discretisation

Mesh Refinement

The accuracy of the trajectory discretisation depends on the number of nodes (mesh density) and the number of collocation points per segment (polynomial order). Increasing the number of segments (and nodes) is referred to as an h-method, and is a technique typically used in direct collocation [38]. A p-method increases the polynomial order by using a greater density of collocation points on each subinterval. Hermite-Simpson collocation is an example of increased order of polynomial splines, assuming quadratic rather than linear splines for the dynamics and control, and cubic splines for the state. Note that the state requires one order higher approximation since it is related to the integral of the control.

2.2.4. Conclusions on Optimal Control Methods

Based on the literature [7, 28, 36, 39], pseudospectral collocation is the most dominant numerical solution method in optimal control. In this method, the state is approximated by a Lagrange polynomial expansion, and system dynamics are enforced at each collocation point.

Pseudospectral transcription can take several forms defining the choice of collocation points. Most commonly, *Legendre-Gauss* (LG), *Legendre-Gauss-Radau* (LGR) and *Legendre-Gauss-Lobatto* (LGL) collocation points are used. These methods determine the distribution of collocation points and whether the interval endpoints are included. An in-depth discussion is provided by Garg et al. [39], and an illustration of the distribution of collocation points is provided in Appendix C. Pseudospectral methods have also been developed to convert the system of dynamic equations into a finite-dimension nonlinear optimisation problem. Common examples are the *Lobatto*, *Gauss* and *Radau* pseudospectral methods. Kaneko and Martins [28] use Radau pseudospectral collocation and LGR nodes in their simultaneous aircraft design and trajectory optimisation.

2.3. MDO Formulation

Multidisciplinary design optimisation (MDO) typically attempts to optimise a finite set of parameters called the *design vector* based on a number of interlinked disciplines which involve analysis of the system. Generally, a single optimisation objective is chosen for minimisation, which may be determined from a combination of outputs from the disciplines. A fundamental difference with OCPs is that an infinite-dimensional trajectory is introduced. Coupling an OCP with a typical MDO problem is therefore a tricky task. Trajectory discretisation, as discussed in Section 2.2.3 on transcription, makes this possible but introduces many more variables than are commonly seen in MDO. Two broad categories of coupling strategies are *nested* and *monolithic* formulations.

Nested MDO methods solve optimisation disciplines sequentially. For example, an outer loop might be responsible for optimising the aircraft design $\boldsymbol{x}_p$ subject to static design constraints only. Within this, an inner loop optimises the trajectory to minimise a certain objective J. This inner loop varies the final time t_f, initial state $\boldsymbol{\xi}_0$ and control $\boldsymbol{u}$ subject to the dynamic, path and boundary constraints. Since the inner loop is a conventional optimal control problem and does not include variables of the physical system or their constraints, it can be implemented with existing libraries [28]. In contrast, monolithic frameworks optimise all problem disciplines simultaneously. They aim to minimise an objective J based on varying time t_f, initial state $\boldsymbol{\xi}_0$, control input $\boldsymbol{u}$ and the physical system $\boldsymbol{x}_p$, all while considering constraints on the system dynamics, the path, initial and final boundaries and the design parameters.

Kaneko and Martins [28] compare these two frameworks in the context of simultaneous aircraft design and trajectory optimisation. They present strong reasons for favouring monolithic frameworks in aircraft trajectory optimisation. First, convergence of a nested framework can fail if aircraft design optimised in the outer loop produces an infeasible problem in the inner loop. They also claim that it is difficult to optimise the outer loop efficiently, since the post-optimality derivatives required must account for the inner loop optimality. The outer loop optimality condition contains second order derivatives, making them difficult to solve. If the post-optimality derivatives are available, they claim that a nested approach is still less efficient since an iterative approach is usually required to solve the inner loop derivatives. Having reasoned that the monolithic architecture was most appropriate, they compared multidisciplinary feasible (MDF) and simultaneous analysis and design (SAND) architectures, concluding that the computational cost of SAND was superior when the trajectory and disciplinary model were directly coupled. If surrogate-based coupling was used, the number of coupling variables is reduced, and the performance of MDF and SAND were similar.

Hwang, Jasa and Martins [29] used an MDF (monolithic) architecture to optimise aircraft design, trajectories and route allocation. Their optimisation contained over 4000 variables and nearly 14000 constraints, displaying the possibility of solving high-fidelity optimisation problems by reformulating them as non-linear programming problems. Yan, Jansen and Perez [31] used MDO to simultaneously optimise aircraft design and trajectory with different objectives. They compare results for optimisations minimising fuel burn, NO_x emissions, weight and cost independently. Although they do not give detail on the MDO formulation used, it appears to be a monolithic framework in which aircraft design and trajectory are optimised in parallel.

2.4. Climate Impact Modelling

The climate impacts of aviation are difficult to predict, particularly due to the uncertainty in the formation and lifetime of contrails and the complex impacts of NO_x. In a recent study widely accepted as the most in-depth on the climate impact of aviation, Lee et al. [3] had low confidence in their estimation of the contributions of contrails and NO_x to radiative forcing. However, they reason that both have significant climate impact. What is clear from this is that our understanding of climate impact in aviation cannot be limited to carbon dioxide emissions. With increased study into these effects, prediction and modelling of contrails is improving. In a validation study Rosenow et al. [40] were able to predict the lifetime of contrails with a 10% margin of error.

To set climate impact as the objective of an optimisation problem, an appropriate metric must be chosen. Megill [11] studied the following climate metrics and their relevance for aviation:

- Radiative Forcing (RF)
- Global Warming Potential (GWP)
- Global Warming Potential Alternative (GWP*)
- Global Temperature-change Potential (GTP)
- Average Temperature Response (ATR)

Radiative forcing (RF) is the flux imbalance between incoming and outgoing radiation from the Earth. Different definitions determine the point in the atmosphere that is measured, and whether the atmosphere, land and/or sea temperatures are allowed to adjust to the new RF. For example, effective radiative forcing (ERF) measures the net flux at the top of the atmosphere while allowing the atmospheric

and land temperatures to adjust, but not the sea. RF is the most basic measure of climate impact, but it is difficult to understand intuitively. Global Warming Potential (GWP) is a measure of global warming effectiveness of certain emission species compared to CO_2. The predicted radiative forcing change of an emission species is integrated up to a certain time horizon H. NO_x, for example, has a GWP 30 times that of the equivalent mass of CO_2 over 20 years [13]. An alternative form, GWP*, improves on this by accounting for Short-Lived Climate Pollutants (SLCP), since the climate rapidly recovers after a decrease in emission rate. Like GWP and GWP*, the global temperature-change potential (GTP) compares emission species to CO_2, but in terms of their absolute global temperature-change potential (AGTP) at an endpoint time H rather than the integrative approach of GWP.

The most appropriate climate metric for aviation is average temperature response (ATR), developed by Dallara, Kroo and Waitz [41], largely because it considers sustained aircraft emissions over a specified period rather than the effect of a pulse emission [11]. In contrast, a 100-year pulse GWP assumes a 1-year pulse emission and none thereafter. Basing the measure on temperature change means it is easily understood by non-experts. ATR is designed to consider the climate impacts that result both during an aircraft lifetime (H) and thereafter. Similar to other climate metrics, it is formulated as

$$\mathrm{ATR}_H = \frac{1}{H}\int_0^\infty \Delta T_{\mathrm{sust},H}(t)w(t)dt \tag{2.19}$$

where $\Delta T_{\mathrm{sust},H}(t)$ is the instantaneous global mean temperature change as a result of the period of sustained emission. It is determined based on emissions of CO_2, NO_x, H_2O, soot, sulphate and the effects of aviation-induced cloudiness (AiC) during the emission period H [41]. AiC is the collective effect of contrails and contrail-induced cirrus (CiC). The original definition of ATR is based on an infinite time integral, but a more practical definition considers a limited time horizon which is generally longer than the emission period. More details on the ATR methods used in this research are given in Section 3.4. Temperature change can be calculated using techniques of varying complexity. Dallara, Kroo and Waitz [41] suggest using linear temperature response (LTR) models as a quick calculation. In application as an optimisation objective (J), Lührs et al. [9] presented the following weighted combination of ATR and direct operating cost (DOC).

$$J = c_\Upsilon \cdot \mathrm{DOC}(t_f - t_0, m_0 - m_f) \cdot \mathrm{DOC}_{\mathrm{ref}}^{-1} + c_\Psi \cdot \underbrace{\left(\sum_i \int_{t_0}^{t_f} \mathrm{CCF}_i(\boldsymbol{x},t)\cdot \dot{m}_i(t)dt + \int_{t_0}^{t_f} \mathrm{CCF}_{\mathrm{CiC}}(\boldsymbol{x},t)\cdot v_{\mathrm{TAS}}(t)dt\right)}_{\mathrm{ATR}_{20,tot}} \cdot \mathrm{ATR}_{20,\mathrm{tot,ref}}^{-1} \tag{2.20}$$

with $i \in \{CO_2, H_2O, NO_x\}$. Weights c_Υ and c_Ψ add to 1, and are both positive. They are adjusted to find the Pareto optimal curve between cost and climate impact. The DOC considered by Lührs et al. [9] includes fuel, crew, maintenance and fees (navigation and landing). The climate cost functions (CCF_i) evaluate the climate impact from an aircraft based on the position, altitude and time of its emissions. Frömming et al. [42] provided an in-depth description of the ECHAM5/MESSY Atmospheric Chemistry model (EMAC) which can be used in this regard.

To encourage airlines to adopt climate optimised routing, some (monetary) incentive might need to be introduced to minimise emissions and time spent in highly climate sensitive regions [15]. One approach commonly suggested is to identify climate sensitive regions and associate a penalty to any trajectory passing through them [25, 43]. This simplifies the problem in that it discretely defines regions to avoid and could lead to practical operational implementation. Ice-supersaturated regions (ISSRs) can somewhat accurately be described this way as isolated areas in which persistent contrails are likely to form. However, it overlooks the continuous nature of climate sensitivity and the fact that there might also be isolated cooling regions which might reduce overall climate impact if flown through [9]. Lim, Gardi and Sabatini [35] developed a trajectory optimisation algorithm to minimise the formation, persistence, and radiative forcing of contrails. They defined the cost associated with atmospheric regions by those that were both supersaturated with respect to ice (ISSRs) and fulfilled the Schmidt-Appleman Criterion (SAC), which evaluates how the aircraft engine exhaust gases cool and condense.

3
Methodology

Modelling and methodology for the optimisation of an aircraft design and flight trajectory is presented in this chapter. To achieve this, the three integral aspects, *trajectory optimisation*, *aircraft design* and *climate impact* are modelled and integrated. Climate impact, operating cost and fuel consumption form the optimisation objectives for comparison cases.

Section 3.1 describes the overall problem structure. This is followed in Section 3.2 by a description of the aircraft parametric design and constraints. Section 3.3 discusses the trajectory setup, initialisation and constraints. The climate model, while inherently a discipline of the trajectory itself, is particularly complex and described separately in Section 3.4. Finally, Section 3.5 describes the main experimental case, defining the baseline atmospheric conditions for the medium range trajectory and the fleet size.

3.1. Problem Structure

The problem is posed as a monolithic multidisciplinary design optimisation (MDO), coupling aircraft design with trajectory optimisation. The Dymos library [37], built on the framework of OpenMDAO, is used to define and optimise trajectories using optimal control theory. The trajectory state and control variables are parameterised with fourth order pseudospectral collocation, as described in Section 2.2.3. Aircraft design variables are statically parameterised, meaning they are optimised alongside the trajectory but remain time-invariant. A full eXtended Design Structure Matrix (XDSM) [44] is presented in Appendix A. As suggested by Kaneko and Martins [28], the general structure of the MDO problem is:

$$\textbf{to minimise:} \quad J(t, \boldsymbol{\xi}(t), \boldsymbol{u}(t), \boldsymbol{x}_p) \tag{3.1}$$

$$\begin{aligned} \textbf{by varying:} \quad & \boldsymbol{\xi}_{\text{LB}} \leq \boldsymbol{\xi}(t) \leq \boldsymbol{\xi}_{\text{UB}} \\ & \boldsymbol{u}_{\text{LB}} \leq \boldsymbol{u}(t) \leq \boldsymbol{u}_{\text{UB}} \\ & \boldsymbol{x}_{p,\text{LB}} \leq \boldsymbol{x}_p \leq \boldsymbol{x}_{p,\text{UB}} \end{aligned} \tag{3.2}$$

$$\begin{aligned} \textbf{subject to:} \quad & \dot{\boldsymbol{\xi}} = \boldsymbol{f}(\boldsymbol{\xi}(t), \boldsymbol{u}(t), t, \boldsymbol{x}_p) \\ & \boldsymbol{g}_{\text{path}}(\boldsymbol{\xi}(t), \boldsymbol{u}(t), t, \boldsymbol{x}_p) \leq \boldsymbol{0} \\ & \boldsymbol{g}_{\text{boundary}}(t_0, t_f, \boldsymbol{\xi}(t_0), \boldsymbol{\xi}(t_f)) \leq \boldsymbol{0} \\ & \boldsymbol{g}_{\text{static}}(\boldsymbol{x}_p) \leq \boldsymbol{0} \end{aligned} \tag{3.3}$$

The objective J in Equation 3.1 takes the form of average temperature response (ATR), direct operating cost (DOC), fuel mass or a combination thereof for comparison. Formulation of the objective is detailed in Section 3.3.3. Equations 3.2 describes the bound values on states $\boldsymbol{\xi}$, controls $\boldsymbol{u}$ and design variables $\boldsymbol{x}_p$. These are detailed in Table 3.2, and apply practical system limits. Equations 3.3 describe the general constraints on the system. The first set describes the system dynamics and is therefore written in terms of the rate of change of the state, $\dot{\boldsymbol{\xi}}$. Path and boundary constraints on the state are described further in Section 3.3.3. In practice, they may also impact convergence of design variables. Static constraints apply to the design variables only.

3.2. Aircraft Parametric Design

The aircraft design module enables optimisation of high-level design variables to complement the trajectory optimisation by integrating them in the optimal control problem as time-invariant parameters. While the methodology is valid for any typical tube-and-wing aircraft, the narrowbody chosen for this study is based on an A320-200 [45] with baseline variables given in Table 3.1. These also serve as the initial values for the aircraft parametric optimisation.

Table 3.1: Aircraft Parametrisation Baseline Values.

	Symbol	Baseline	Unit
Design Variables			
Engine Bypass Ratio	BPR	11.0	-
Wing Aspect Ratio	A	10.45	-
Wing Loading	W/S	5881	N/m^2
Wing Sweep	Λ_{qc}	25.0	deg
Dependent Variables			
Wing Area	S	122.6	m^2
Wing Span	b	35.8	m
Approach Wing Loading	W/S_{approach}	5161	N/m^2
Buffet Lift Coefficient	$C_{L_{\text{buffet}}}$	0.779	-
Max. Lift Coefficient	$C_{L_{\text{max}}}$	2.54	-
Fixed Variables			
Max. Takeoff Mass	MTOM	73 500	kg
Max. Landing Mass	MLM	64 500	kg
Operating Empty Mass	m_{OE}	42 400	kg
Payload Mass	m_{pay}	*	kg
Reserve Fuel Mass	$m_{\text{fuel,res}}$	**	kg

*Payload mass is case dependent. See Section 3.5.
**Reserve fuel mass is assumed 1300 kg plus 750 kg per 1000 km of expected range.

To ensure a feasible aircraft design in the parametric aircraft optimisation, several constraints are applied. For this, the dependent variables appearing in Table 3.1 are derived from the design variables. The surface area (Eqn. 3.4) and wing span (Eqn. 3.5) are determined from the wing loading, aspect ratio and design maximum takeoff mass (MTOM). The approach wing loading, W/S_{approach}, in Equation 3.6 is derived from the design maximum landing mass (MLM). Maximum lift coefficients during cruise (Eqn. 3.7) and approach (Eqn. 3.8) are estimated from the quarter-chord sweep (Λ_{qc}). These simple assumptions are based on experimental lift polar data of commercial aircraft studied by Obert [46].

$$S = \frac{\text{MTOM} \cdot g}{W/S} \tag{3.4}$$

$$b = \sqrt{\text{AR} \cdot S} \tag{3.5}$$

$$W/S_{\text{approach}} = \frac{\text{MLM} \cdot g}{S} \tag{3.6}$$

$$C_{L_{\text{buffet}}} = 0.86 \cdot \cos \Lambda_{qc} \tag{3.7}$$

$$C_{L_{\text{max}}} = 2.9 \cdot \cos \Lambda_{qc} \tag{3.8}$$

The design constraints include an upper limit on the lift coefficient during cruise to avoid buffet (Eqn. 3.9). The second constraint (Eqn. 3.10) limits the allowable wing loading during the approach to landing. The effect of wing sweep on both the buffet onset and maximum lift coefficients makes it an interesting design variable to consider. A minimum allowable approach speed of v_{app} of 70 m/s is assumed. Approach conditions assume a standard sea-level air density ρ_0 of 1.225 kg/m^3. A wing

span constraint b_{max} of 36 m ensures that the aircraft adheres to sizing category III (Eqn. 3.11). Since the buffet constraint is relevant to every point on the trajectory it is applied as a path constraint and $C_{L_{\text{cr}}}$ is taken as the lift coefficient at each trajectory node. The approach and wing span constraints are static design constraints. Bounds are applied to the design variables in the same way as to state and control variables to ensure a consistent aircraft design. These are shown in Table 3.2.

$$C_{L_{\text{cr}}} \leq \frac{C_{L_{\text{buffet}}}}{1.3} \tag{3.9}$$

$$W/S_{\text{approach}} \leq \frac{1}{2}\rho_0 \left(\frac{v_{\text{app}}}{1.23}\right)^2 C_{L_{\text{max}}} \tag{3.10}$$

$$b \leq b_{\text{max}} \tag{3.11}$$

3.3. Trajectory Optimisation

This section describes each of the modules which define the trajectory, including atmospheric conditions, aerodynamic forces, propulsion modelling and system dynamics, as well as the constraints and objectives for which the trajectory is optimised. Including the aircraft design parametrisation and climate impact modules brings together the full optimisation problem.

3.3.1. Trajectory Definition

The aircraft trajectory is transcribed using pseudospectral collocation, based on strong literature support for its appropriateness to aircraft trajectory optimisation problems [7, 28, 36, 39]. The continuous trajectory states are discretised by a series of nodes, and approximated by interpolating functions which are fitted to collocation points, as represented in Figure 3.1. For medium range cases of 4000km (see Section 3.5), 12 trajectory nodes are used, whereas short range cases of 2000km were transcribed with 6 nodes. Fourth order Legendre-Gauss-Radau collocation points were used on the interval between nodes (see Appendix C). The design vector $\boldsymbol{z}(t)$ contains each state as well as the adjoints which are used to apply system constraints (see Section 2.2.3).

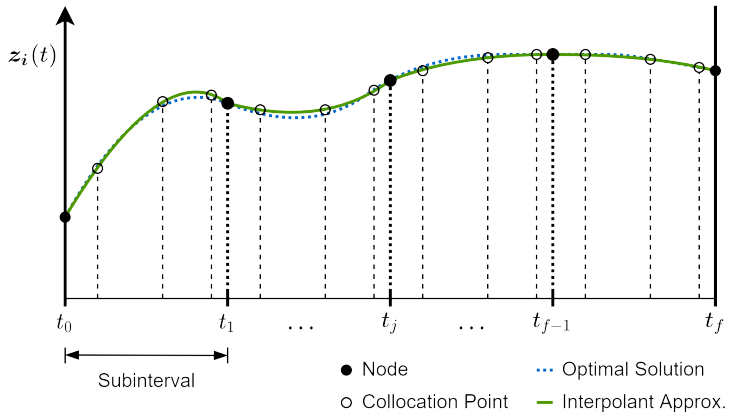

Figure 3.1: Fourth Order Legendre Gauss Radau Transcription

The benchmark trajectory is the cost-optimal solution based on the standard reference aircraft (Table 3.1). The trajectory consists of states $\boldsymbol{\xi}$, controls $\boldsymbol{u}$ and design variables $\boldsymbol{x_p}$, as shown in Equation 3.2. The components of these are defined in Table 3.2, which provides normalisation reference values and bounds for each variable. The design vector is normalised to aid the optimiser as it searches the design space by modifying each variable proportionally to this value. The stability and speed of optimisation convergence can be very sensitive to the values provided. Generally, a reference value of similar order to the parameter itself provides good results. For variables such as flight distance with a large range of expected values, convergence could be improved with smaller reference values, closer to the expected variation between trajectory nodes.

Table 3.2: Trajectory Variable Definitions, Normalisation References and Bounds.

Variable Name	Symbol	Normalisation Reference	Lower Bound	Upper Bound	Unit
Controls					
Angle of Attack	$\boldsymbol{\alpha}$	1	-1	8	deg
Turbine Entry Temp.	$\boldsymbol{T_{t4}}$	1000	-	1700	K
States					
Altitude	$\boldsymbol{h}$	500	500	13500	m
Aircraft Mass	$\boldsymbol{m}$	30×10^3	$m_{\text{OE}} + m_{\text{pay}}$	MTOM	kg
Flight Distance	$\boldsymbol{r}$	100	0	-	km
Airspeed	$\boldsymbol{v}$	100	150	280	m/s
Flight Path Angle	$\boldsymbol{\gamma}$	2	-3	3	deg
ATR	**ATR**	$8 \cdot 10^{-4}$*	-	-	K
Design Variables					
Engine Bypass Ratio	BPR	5	6	11	-
Wing Aspect Ratio	A	5	6	13	-
Wing Loading	W/S	3000	4000	8000	N/m^2
Wing Sweep	Λ_{qc}	10	0	40	deg

*Determined based on an expected total ATR of 10-20 mK. A small normalisation value appears to help the optimiser to determine the contributions from each species, since some have a far smaller effect than others.

3.3.2. Disciplinary Analysis

The trajectory is built from a number of disciplines to model each aspect of the aircraft flight. Figure 3.2 displays each discipline, their required inputs, dependencies and outputs for the optimiser and constraint handling. Referring to the trajectory transcription (Section 2.2.3), the states and controls are passed to the optimiser after being discretised by the trajectory nodes. Definitions of hidden variables in the XDSM - those not part of the state, control or design variables - can be found in Table 2.

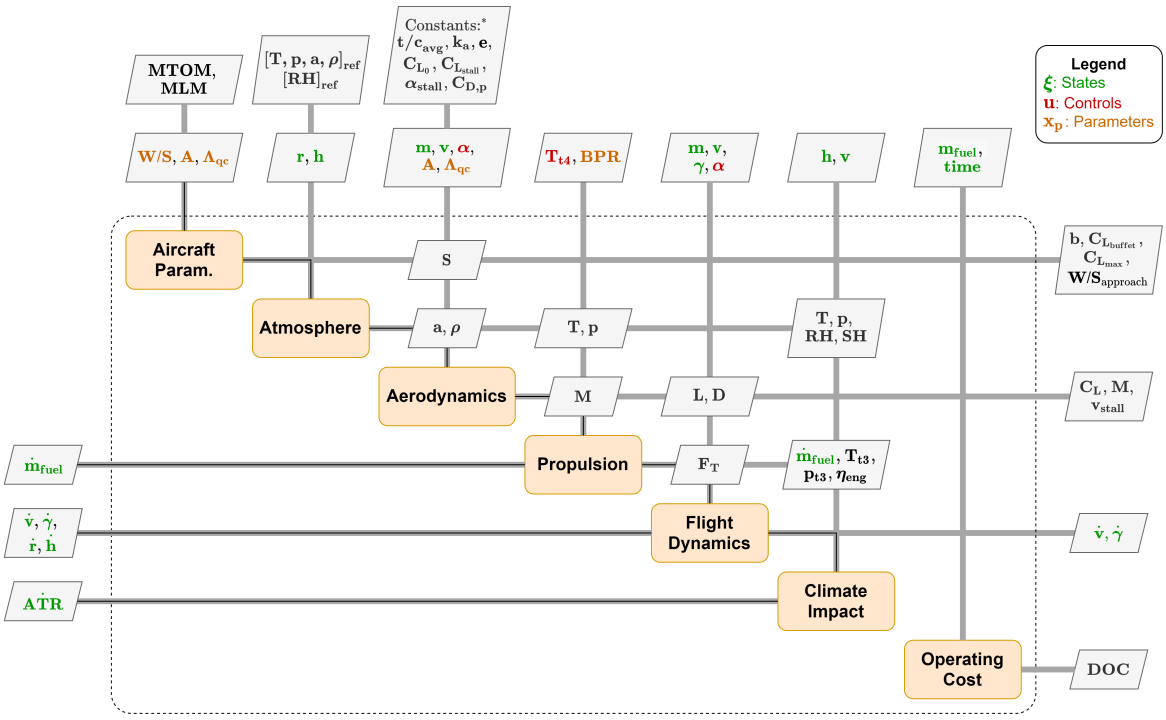

Figure 3.2: Trajectory Discipline Structure

Atmosphere Discipline

The atmosphere discipline defines properties of the flight environment that affect aerodynamics, propulsion, emissions rates and climate impacts. The structure is shown in Figure 3.3. Most properties are interpolated from average reference values based on a 1976 U.S. Standard Atmosphere [37]. Relative humidity is more variable, but experimental data from Held [47] is used. This module is important because the NO_x emission rate and contrail formation properties depend on atmospheric humidity and temperature. Variations are added to the humidity along the flight path distance, thereby creating a representative atmosphere containing regions in which contrails will form and others which are unaffected. In Section 3.5, the baseline atmosphere case is shown and humidity variations are visualised.

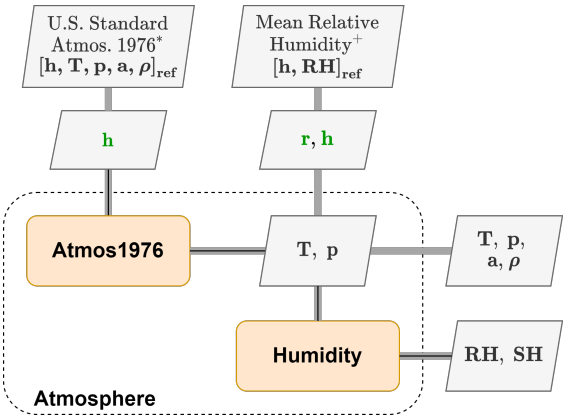

Figure 3.3: Atmosphere Discipline Structure
*1976 U.S. Atmosphere Data [37], +Mean Relative Humidity with Altitude [47]

Aerodynamics Discipline

The aerodynamics discipline determines the aircraft lift and drag polars and aerodynamic forces used to update the state. Figure 3.4 displays the discipline structure.

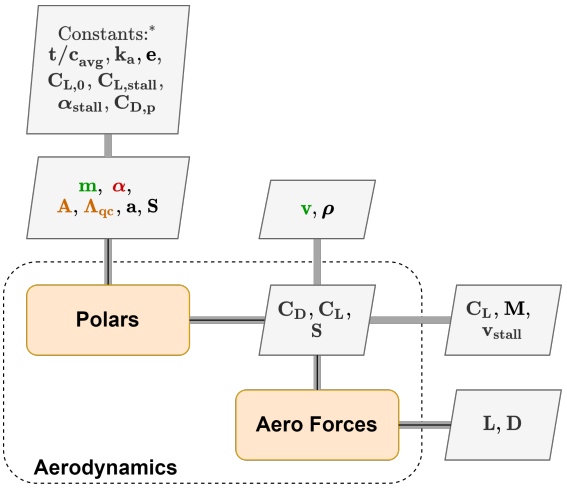

Figure 3.4: Aerodynamics Discipline Structure
*Geometric values assumed constant

The lift polar (Eqn. 3.12) is assumed linear between a zero-incidence lift coefficient of 0.3 and a maximum lift coefficient of 1.5 at a 7 degree angle of attack. These values were inferred from Airbus A320 lift curve data from Sun, Ellerbroek and Hoekstra [48] and an narrowbody aerodynamics example model from Falck et al. [37].

$$C_L = C_{L_0} + \frac{\alpha}{\alpha_{\text{max}}} \left(C_{L_{\text{max}}} - C_{L_0} \right) \tag{3.12}$$

The drag polar is composed of zero-lift, lift-induced and wave drag components, C_{D_0}, C_{D_l} and C_{D_w}, respectively. Zero-lift drag (Eqn. 3.13) includes parasitic drag, size-dependent and size-independent excrescence drag $C_{D_{p,min}}$, $\Delta C_{D_{E,I}}$ and $\Delta C_{D_{E,II}}$, respectively. The parasitic drag coefficient is assumed 0.0175, based on the low Mach number performance curves of an A320 by Sun, Ellerbroek and Hoekstra [48], and size independent excrescence drag is assumed to add 1.5% to this. Size-independent excrescence drag is assumed to be $0.035/S$, as was assumed by Proesmans and Vos [1]. The lift-induced drag coefficient has a quadratic relation to the lift coefficient as given by Equation 3.14. The Oswald factor e is assumed 0.8.

The wave drag coefficient C_{D_w} is estimated by the extended Korn equation (3.15) while the drag-divergence mach number M_{dd} is given by Equation 3.16 [49]. Drag divergence depends on the quarter-chord sweep angle Λ_{qc}, and constants relating to the airfoil design. The airfoil technology factor k_a is assumed 0.935 and the thickness-to-chord ratio t/c_{avg} is taken as 0.12. The critical lift coefficient $C_{L_{crit}}$ describes the lift coefficient of the most critical wing section. It is assumed that the overall wing lift coefficient $C_{L_{wing}}$ is 10% lower than $C_{L_{crit}}$. The wing lift coefficient is further assumed 3% higher than that of the full aircraft, therefore $C_{L_{crit}} = 1.03/0.9 \cdot C_L$.

$$C_{D_0} = C_{D_{0,p}} + \Delta C_{D_{E,I}} + \Delta C_{D_{E,II}} \tag{3.13}$$

$$C_{D_l} = \frac{1}{\pi \cdot A \cdot e} \cdot C_L^2 \tag{3.14}$$

$$C_{D_w} = 20 \cdot \left(M - M_{dd} + \left(\frac{0.1}{80} \right)^{\frac{1}{3}} \right)^4 \tag{3.15}$$

$$M_{dd} = \frac{k_a}{\cos \Lambda_{qc}} - \frac{t/c_{avg}}{\cos^2 \Lambda_{qc}} - \frac{C_{L_{crit}}}{10 \cos^3 \Lambda_{qc}} \tag{3.16}$$

Propulsion Discipline

Appropriate for the baseline narrowbody aircraft, thrust is provided by two high-bypass twin-spool turbofans with design parameters matched closely to the state-of-the-art CFM Leap-1A engine, as used by A320-200 aircraft. As described in the trajectory definition (Sec. 3.3.1), turbine entry temperature (T_{t4}) is a control variable, while the bypass ratio is a design parameter. An analytical surrogate model was developed to closely match that developed by Proesmans and Vos [1], which employed techniques from Mattingly, Heiser and Pratt [50]. Table 3.3 provides the design values of the reference engine. Note that while T_{t4} is used as the trajectory throttle control, the engine is designed to operate best at $T_{t4,design}$ which is a fixed parameter.

Table 3.3: Engine Design Parameters. Assumptions are based on the propulsion model by Proesmans and Vos [1] and material from the AE4238 Aero Engine Technology course (TU Delft).

Design Parameters	**Value**	**Unit**
Total Air Mass Flow	173	kg/s
Design Turbine Entry Temp. ($T_{t4,design}$)	1480	K
Static Temperature	216.65	K
Static Pressure	22631.7	Pa
Fan Pressure Ratio	1.4	-
LPC Pressure Ratio	1.4	-
HPC Pressure Ratio	27.0	-
Design Assumptions	**Value**	**Unit**
Fan Polytropic Efficiency	0.915	-
Compressor Polytropic Efficiency (LP & HP)	0.9	-
Turbine Polytropic Efficiency (LP & HP)	0.93	-
Inlet Pressure Ratio	0.98	-
Combustor Pressure Ratio	0.96	-

Outputs of the propulsion discipline are thrust, fuel consumption, total efficiency, and temperature and pressure ahead of the combustor, T_{t3} and p_{t3}, respectively. Engine efficiency is required for contrail formation properties, while T_{t3} and p_{t3} are used to determine the emissions index of NO_x (Eqn. 3.18). Verification of the propulsion surrogate model is shown in Appendix D.

Flight Dynamics Discipline

A simple 2-dimensional flight dynamics model is used to determine the aircraft state evolution. Outputs are the rates of change of velocity $\dot{v}$, flight path angle $\dot{\gamma}$, altitude $\dot{h}$ and horizontal distance $\dot{r}$ as given by equations 3.17. Figure 3.5 displays the aerodynamic lift (L) and drag (D), and the gravitational force (F_G). Thrust (F_T) is assumed to align with the aircraft body axes (shown in red). The flight path angle (γ) and angle of attack (α) are also shown.

$$\begin{aligned}
\dot{v} &= \frac{F_T \cdot \cos\alpha - D}{m} - g \cdot \sin\gamma \\
\dot{\gamma} &= \frac{F_T \cdot \sin\alpha + L}{m \cdot v} - \frac{g}{v} \cdot \cos\gamma \\
\dot{h} &= v \cdot \sin\gamma \\
\dot{r} &= v \cdot \cos\gamma
\end{aligned} \tag{3.17}$$

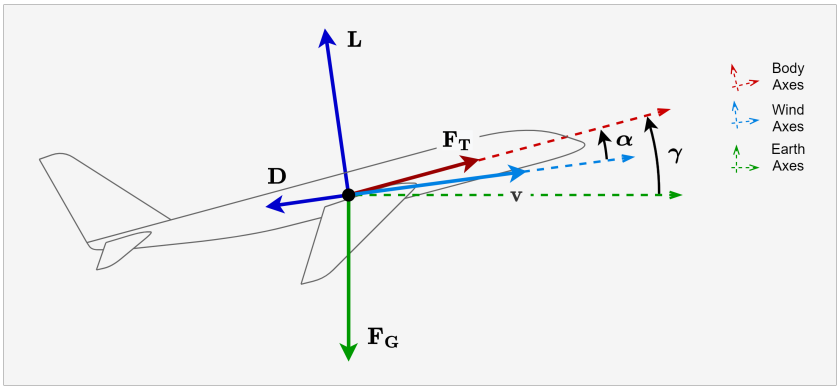

Figure 3.5: Flight Dynamics Force Diagram

Emissions and Climate Discipline

The climate effect of a flight, measured in ATR_{100}, is determined using an emissions and climate effects module, the structure of which is shown in Figure 3.6.

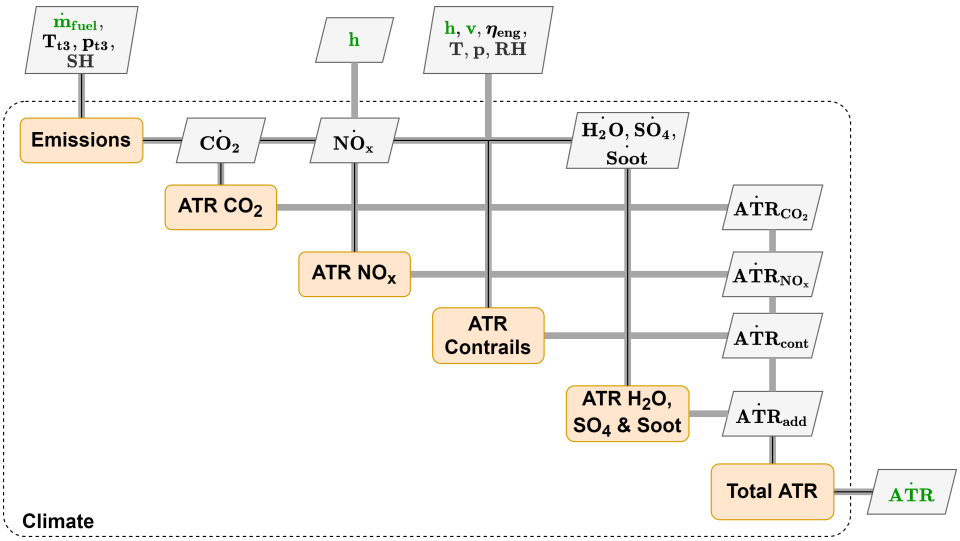

Figure 3.6: Emissions and Climate Discipline

The considered emissions are carbon dioxide (CO_2), nitrogen oxides (NO_x), water vapour (H_2O), sulphates (SO_4) and soot. Emissions are determined from the species emission index (EI), which indicates the mass of pollutant that is produced per kilogram of fuel burned. These emission indices are mostly assumed constant, as provided in Table 3.4, and are multiplied by the fuel flow to find the emission rate. NO_x emissions depend on engine operating conditions and atmospheric specific humidity H_0 [51], as shown in Equation 3.18.

Table 3.4: Emission Indices [41].

Species	CO_2	H_2O	SO_4	Soot
EI_i (kg/kg)	3.16	1.26	2.0×10^{-4}	4.0×10^{-4}

$$EI_{NO_x} = 0.0986 \cdot \left(\frac{p_{T3}}{101325}\right)^{0.4} \cdot \exp\left(\frac{T_{T3}}{194.4} - \frac{H_0}{53.2}\right) \tag{3.18}$$

Section 3.4 is dedicated to the methodology used to estimate the ATR resulting from these emissions.

Direct Operating Costs

Direct operating costs (DOC) are composed of crew salaries, time-dependent maintenance costs and fuel costs. Airbus's cost indexing guide from 1998 [52] suggested crew costs at 5-10 $/min. Taking the mean and accounting for 93% inflation[1], total crew rates for narrowbody aircraft are assumed at $14.5/min. This also roughly correlates with the €25/min crew costs for widebody aircraft assumed by Grewe et al. [15] in 2017. Time-dependent maintenance costs are assumed at $7/min. Airbus's suggested range for maintenance costs in 1998 [52] was 3-7 $/min. It was assumed that maintenance costs did not inflate as much as crew costs due to technological improvements extending component life and reliability. The latest fuel price (September 2024) of 0.70 $/kg was taken from the International Air Transport Association (IATA)[2]. Using flight time and fuel consumption, the total DOC is easily estimated.

3.3.3. Objective and Constraints

The objective and constraints are added to the design structure matrix as shown in Figure 3.7.

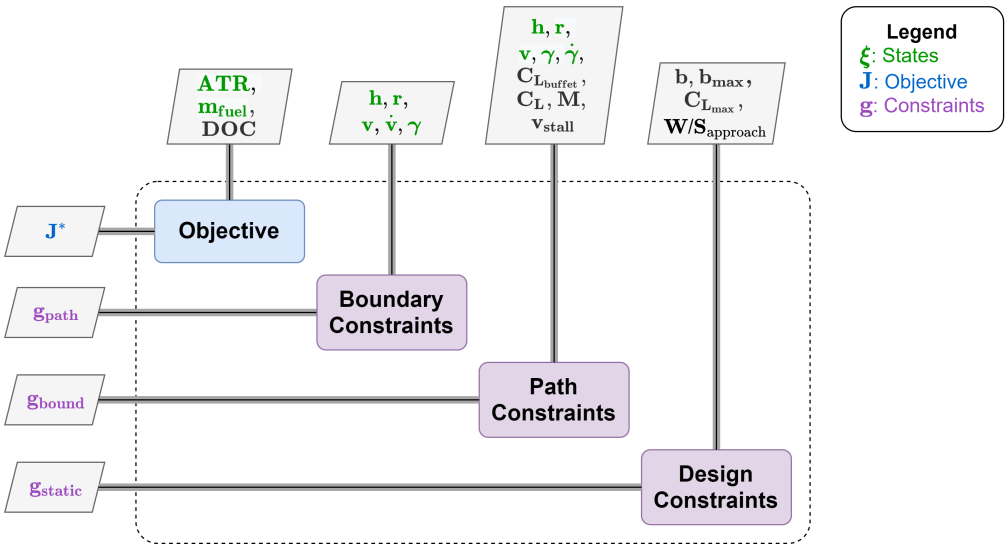

Figure 3.7: Trajectory Objective and Constraints

[1] https://www.in2013dollars.com/us/inflation/1998?amount=1
[2] https://www.iata.org/en/publications/economics/fuel-monitor/

Objective

The objective defines the minimisation goal of the trajectory and aircraft optimisation. In this study, DOC and ATR are of interest, and are weighted in the objective using cost and climate weightings, ψ_c and ψ_a respectively. This is used to develop compound objective, as formulated by Lührs et al. [9] (Equation 3.19). In this way, the importance of DOC in relation to ATR_{100} can be chosen by setting a ψ_c value between 0 and 1. A cost-optimal trajectory corresponds to a cost weighting of 1, while an 0-weighting will result in an ATR-optimal trajectory. DOC_{ref} and $ATR_{100,ref}$ are the respective values associated with a cost-optimal trajectory and baseline aircraft design.

$$J = \psi_c \cdot \frac{DOC}{DOC_{ref}} + \psi_a \cdot \frac{ATR_{100}}{ATR_{100,ref}} \tag{3.19}$$

where:

$$\psi_c + \psi_a = 1$$

In the optimisation process, NO_x impacts proved very complex due to the combination of ATR-positive short-term ozone impacts and ATR-negative long-term methane impacts, which, when combined can have a net positive or negative ATR depending on emission altitude. This results in an oscillatory optimal trajectory and incomplete convergence, while having little improvement in the ATR impact. A more in-depth description is given in the recommendations Section 6.3.2. It was concluded for this study that the nitrogen oxide impact would be excluded from the objective. However, the effects of NO_x are considered in all presented ATR values.

Constraints

Constraints define the trajectory end-points and apply restrictions to the allowable path. The objective and constraints are added to the extended design structure matrix (XDSM) as shown in Figure 3.7. The relevant path and boundary constraints are given in Table 3.5. Design parameter constraints are added in the same way. Path bounds on the airspeed rate $\dot{v}$ were added to limit oscillations in the trajectory results and were decided based on preliminary results to allow as much freedom as possible while maintaining smooth behaviour. Typically for high cost-weighted trajectories, the airpseed rate bounds were reached only on the first and last nodes, with the remainder well within the allowable range (a maximum seen in contrail avoidance manoeuvres is almost two orders of magnitude smaller than the bounds). Bounds on the flight path angular rate $\dot{\gamma}$ were added for a similar reason. Although they did not become active in any optimised cases, they appeared to aid convergence by limiting the optimisation space. The maximum achieved final value of was roughly half the bounded value.

Table 3.5: Trajectory Path & Boundary Constraints.

Variable	Lower Path Constraint	Upper Path Constraint	Initial Condition	Final Condition	Unit
Altitude h	-	-	1000	1000	m
Mach Number* M	-	0.9	-	-	-
Flight Distance r	-	-	0	range**	km
Thrust* T	0.0	-	-	-	N
Airspeed v	-	-	150	150	m/s
Airspeed Rate* $\dot{v}$	-0.15	0.15	-	0	m/(s^2)
Flight Path Angle γ	-	-	-	≥ -3.0	deg
F.P. Angular Rate* $\dot{\gamma}$	-0.01	0.01	-	-	deg/s

*These constraints form part of g_{path} in Equation 3.3.
**Range is case dependent. See Section 3.5.

3.4. Climate Impact Measurement

3.4.1. Temperature Response to Fleet Emissions

Accurate prediction of the climate impact of an aircraft or fleet is necessary for meaningful optimisation of an aircraft and its trajectory. The ATR is determined using flight emission rates and local atmospheric conditions. Initially proposed by Dallara, Kroo and Waitz [41] (Eqn. 2.19), the ATR_H is the global near-surface temperature response due to emissions averaged over a lifetime H, as shown in Figure 3.8.

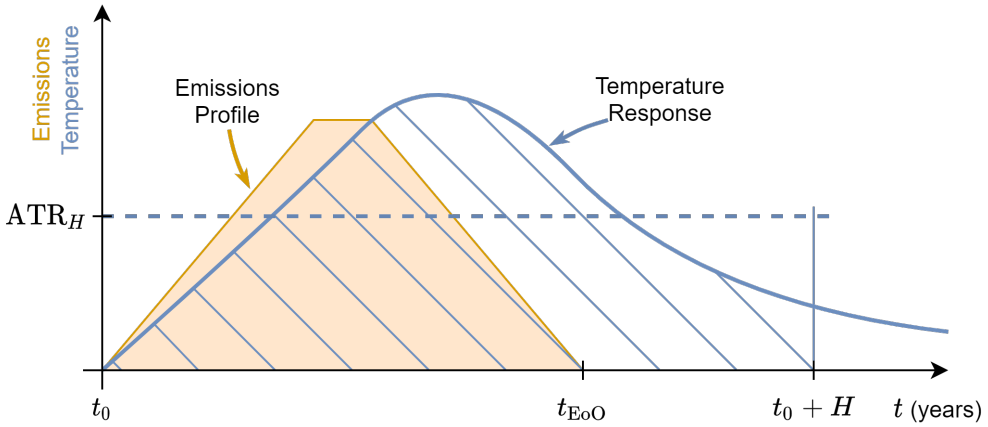

Figure 3.8: Illustration of ATR Calculation: Temperature response is integrated over the period of interest H as a result of aircraft emissions from entry into service (t_0) until end-of-operations (EoO).

The emissions period, from entry into service (t_0) until end-of-operations (t_{EoO}), is typically shorter than H and can include ramp-up as new aircraft are introduced to a fleet and ramp-down as they retire. Here, the fleet profile methodology of Proesmans and Vos [1] is followed for reasonable comparison. In their work, the fleet size is assumed to grow over 30 years, peaking at 17 million flights per year. After a 35 year lifetime, aircraft begin retiring and the total number of flights linearly decreases. A 100-year temperature response period is taken, giving the ATR_{100}.

Emissions contributions from carbon dioxide (CO_2), nitrogen oxides (NO_x), water vapour (H_2O), sulphates (SO_4), soot and linear contrails are considered. Emissions rates are determined in the propulsion module described in Section 3.3.2. NO_x is not a greenhouse gas itself, but leads to long-term depletion of methane (CH_4) and ozone (O_3) and short-term production of ozone. These effects are referred to as NO_x-CH_4, NO_x-O_{3L} and NO_x-O_{3S}, respectively.

3.4.2. Climate Response Modelling

Calculation of ATR creates the link between aircraft emissions and the climate response. Because the climate impact depends on atmospheric conditions and the location that certain emission species are produced, ATR cannot be calculated from the cumulative emissions of a flight. Instead, the impact at each trajectory node is considered by modelling the ATR as a *rate* ($\dot{\text{ATR}}_H$ in Eqn. 3.20), based on emission rates (and airspeed for contrails) at each trajectory node, rather than cumulative emissions (and total distance). This is equivalent to breaking up the flight into individual segments and adding the resulting ATR from each segment, but assuming these segments last just one second (the base unit of time). ATR is then modelled as Dymos state, for which the ATR rate is integrated. A similar method was used by Lührs et al. [9], where the climate response was determined as a rate, and only then integrated over the flight time, as shown in Equation 2.20. Calculations are much the same as for a standard ATR calculation, except that the concentration perturbations, radiative forcing effects (Eqn. 3.22) and temperature response (Eqn. 3.21) from each species are determined as a rate per second of flight time (note overdot notation indicates a rate with respect to trajectory time variable t).

$$\dot{\text{ATR}}_H = \frac{1}{H_{\text{ATR}}} \int_0^H \Delta\dot{T}(t)dt \tag{3.20}$$

$$\Delta\dot{T}(t) = \int_{t_0}^{t} G_T(t-t') \cdot \dot{\mathrm{RF}}^*(t')dt' \tag{3.21}$$

$$\dot{\mathrm{RF}}^*(t) = \sum_{i}^{\text{all species}} \left[f_i \cdot \frac{\dot{\mathrm{RF}}_i(t)}{\mathrm{RF}_{2\times \mathrm{CO_2}}} \right] \tag{3.22}$$

for i =CO_2, NO_x-CH_4, NO_x-O_{3L}, NO_x-O_{3S}, H_2O, SO_4, soot and linear contrails. Climate efficacy f_i (Table B.2) is a normalising factor relating the climate sensitivity of each species to that of CO_2.

Carbon Dioxide

As carbon dioxide is a long-lived greenhouse gas, the atmospheric perturbation from a single emission (either a pulse or a function of time) must be convoluted (Eqn. 3.23) with a climatic response function $G_{\chi_{\mathrm{CO_2}}}$, which describes the decay of the perturbation over time (see Appendix B for details). Sausen and Schumann [53] provide a response function for this, which was validated by Proesmans and Vos [1]. Note that this differs from the original perturbation equation in that it determines perturbation rate $\Delta\dot{\chi}_{\mathrm{CO_2}}$ from the emission rate $\dot{E}_{\mathrm{CO_2}}$, rather than in absolute terms.

$$\Delta\dot{\chi}_{\mathrm{CO_2}}(t) = \int_{t_0}^{t} G_{\chi_{\mathrm{CO_2}}}(t-t') \cdot \dot{E}_{\mathrm{CO_2}}(t')dt' \tag{3.23}$$

The radiative forcing effect of CO_2 (again, as a rate per second of flight time) is a function of the perturbation rate and its background concentration $\chi_{\mathrm{CO_2},0}$, assumed to be 380 ppmv.

$$\dot{\mathrm{RF}}^*_{\mathrm{CO_2}}(t) = \frac{1}{\ln 2} \cdot \ln\left(\frac{\chi_{\mathrm{CO_2},0} + \Delta\dot{\chi}_{\mathrm{CO_2}}(t)}{\chi_{\mathrm{CO_2},0}} \right) \tag{3.24}$$

Nitrogen Oxides

Emissions of nitrogen oxides have long-term depletion effects on methane and ozone, thereby leading to a cooling effect, that is, a *negative* radiative forcing. It also leads to a short-term increase in ozone, creating a warming effect more significant than CO_2 [3].

Methane & Long-Term Ozone

Like CO_2, the effects of methane and long-term ozone are modelled with a perturbation response function.

$$\dot{\mathrm{RF}}_{\mathrm{i}}(t,h) = s_i(h) \int_{t_0}^{t} G_i(t-t') \cdot \dot{E}_{\mathrm{NO_x}}(t')dt' \tag{3.25}$$

Unlike CO_2, nitrogen oxides do not diffuse quickly through the atmosphere, and the climate response to methane and ozone differs with altitude. This is accounted for with a forcing function $s_i(h)$, obtained from Dallara, Kroo and Waitz [41]. The response function $G_i(t)$ accounts for the radiative forcing sensitivity of CH_4 and O_{3L} using values $\mathrm{RF}/\mathrm{E}_{\mathrm{ref}_i}$ from Appendix Table B.2. Perturbation lifetime is assumed to be 12 years.

Short-Term Ozone

The radiative effect of short-term ozone is modelled more simply as:

$$\dot{\mathrm{RF}}_{\mathrm{NO_x\text{-}O_{3S}}}(t,h) = s_{\mathrm{NO_x\text{-}O_{3S}}}(h) \cdot \left(\frac{\mathrm{RF}_{\mathrm{ref}}}{E_{\mathrm{ref}}} \right)_{\mathrm{NO_x\text{-}O_{3S}}} \cdot \dot{E}_{\mathrm{NO_x}}(t) \tag{3.26}$$

Again, an altitude forcing factor $s(h)$ is applied for NO_x-O_{3L} [41], and its reference radiative forcing sensitivity $\mathrm{RF}/\mathrm{E}_{\mathrm{ref}}$ is given in Table B.2

Contrails

Persistent contrails form when water vapour from the engine exhaust condenses and freezes. The layer of droplets contribute to the greenhouse effect by trapping terrestrial radiation. For contrails to persist, three criteria must be satisfied. First, the Schmidt-Applemann Criterion (SAC) is used to determine whether contrails will initially form. This occurs if the exhaust reaches saturation point with respect to

water as it mixes with the ambient air. Second, the condensation must freeze, which occurs below -38°C. Finally, contrails persist only if the mixed and cooled exhaust has a partial vapour pressure above the saturation point with respect to ice, which is determined using formulation by Sonntag [54]. For each node in the trajectory, the three criteria are evaluated to determine if contrails will persist. If they do, the following radiative forcing rate is applied to that node:

$$\dot{\mathrm{RF}}_{\mathrm{con}}(t,h) = s_{\mathrm{con}}(h) \cdot \left(\frac{\mathrm{RF}_{\mathrm{ref}}}{L_{\mathrm{ref}}}\right)_{\mathrm{con}} \cdot v(t) \tag{3.27}$$

Like methane and ozone, the altitude at which contrails form impacts their radiative forcing effect. This is accounted for by the factor $s_{\mathrm{con}}(h)$ [41], which is included in the appendix. The reference radiative forcing effect per contrail kilometer $\mathrm{E}_{\mathrm{ref}}$ is multiplied by the aircraft velocity (in km/s) to obtain the radiative forcing rate.

The formation criteria, however, result in a binary nature for contrail persistence - a strong assumption to make considering atmospheric mixing effects and uncertainties in the conditions. More critically for this work, if a trajectory optimiser is to avoid a contrail region, it requires a gradient of varied impact resulting from a contrail depending on its proximity to a region in which contrails persist. To implement this, a weighting is included on each persistence criterion mentioned above, depending on the proximity to satisfaction of that condition. This can be understood either as a varied climate impact from a contrail which forms or as the likelihood of a contrail forming in that region to begin with, which, for a large number of flights passing through the same conditions, would lead to an equivalent total climate impact. For example, a 30% contrail formation likelihood could mean that a contrail in that regions has an RF of 30% of that given by Equation 3.27, or that 30% of the aircraft flying through those conditions would create a full contrail and others would create none. Persistence weighting for the freezing criterion is illustrated in Figure 3.9, where a hyperbolic tangent function is used to smooth the transition from *no impact* to *full contrail impact*.

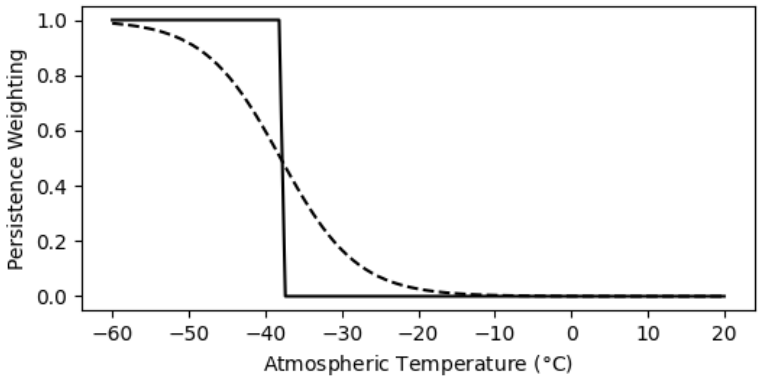

Figure 3.9: Persistence Weighting Variation with Temperature for Contrail Freezing Criterion.

Water Vapour, Sulphates & Soot

Similar to short-term ozone, water vapour, sulphates and soot impact global radiative forcing in the short term. Altitude dependency is not considered.

$$\dot{\mathrm{RF}}_i(t) = \left(\frac{\mathrm{RF}_{\mathrm{ref}}}{E_{\mathrm{ref}}}\right)_i \cdot \dot{E}_i(t) \text{ for } \mathrm{H_2O},\ \mathrm{SO_4} \text{ \& soot} \tag{3.28}$$

3.5. Experimental Setup

The focus of this study is a 4000km flight route with atmospheric conditions varied along the flight path as shown in Figure 3.10. The baseline for comparisons between different objectives and aircraft cases (baseline or optimised) is taken as the cost-optimal trajectory for the baseline narrowbody aircraft design as defined in Table 3.1. Atmospheric humidity varies with altitude based on experimental data from Held [47], impacting the contrail persistence properties and NO_x emissions. Horizontal humidity variation is selected to provide interesting conditions for an ATR-optimal trajectory, testing the ability of the optimiser to avoid a contrail persistence region (CPR) after reaching cruise altitude, and return again to cruise before the descent phase. The case roughly matches a typical medium range mid-latitude flight based on the percentage of flight distance in which contrails are expected to persist [8]. The contribution fraction of contrails to the climate impact for a cost optimal flight is also comparable to that presented by Lee et al. [3], although it is noted that this reference measures climate impact in ERF and not ATR. The humidity variation is described in more detail in Appendix F.

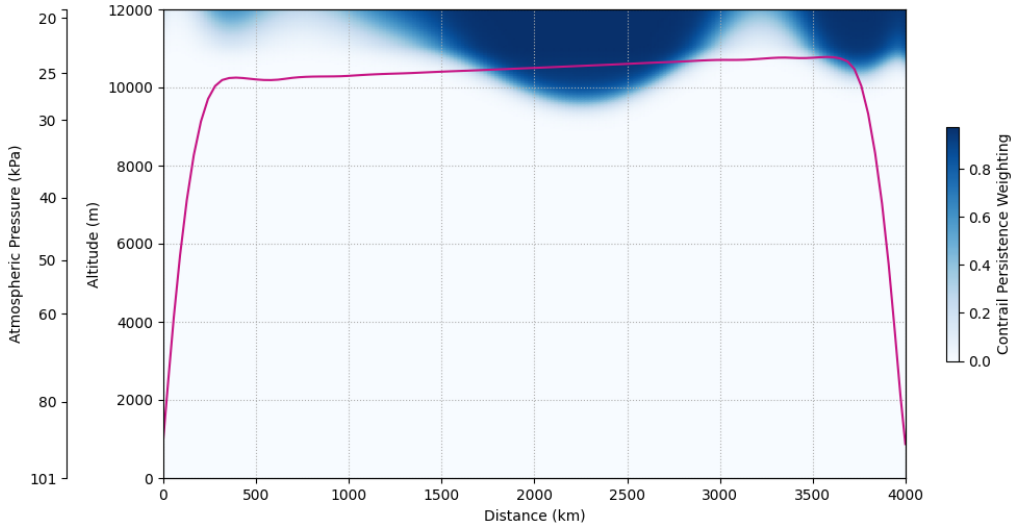

Figure 3.10: Baseline Cost-Optimal Trajectory for Medium Range Case.

Slightly different cases are introduced to evaluate the effect of alternative atmospheric conditions and a short range route of 2000km (see Results Sections 4.5 and 4.6). The payload carried in each case corresponds to the maximum allowable based on the payload-range diagram of an A320-200 [45]. For a 4000km flight this is 16 tons, whereas an 18-ton load can be carried for a 2000km flight.

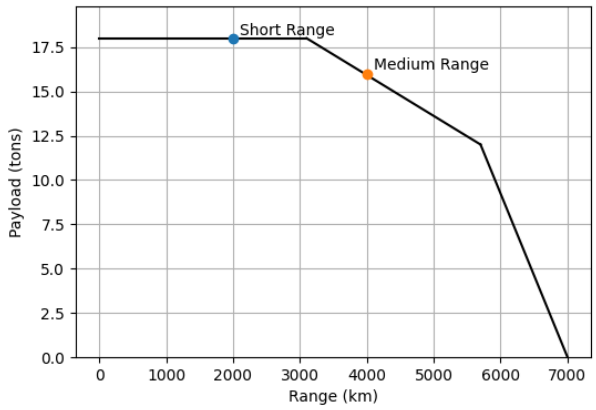

Figure 3.11: Payload Range Diagram of an A320-200 Aircraft [45] with Short and Medium Range Cases.

As the ATR is dependent on an emissions profile rather than a single flight, the fleet is defined as in Figure 3.12. A 30-year aircraft production period is assumed, where the number of flights linearly

increases to a peak of 17 million flights per year. After 35 years, aircraft are retired, giving the fleet a total lifetime of 65 years. A total of 620 million flights occurs during this period.

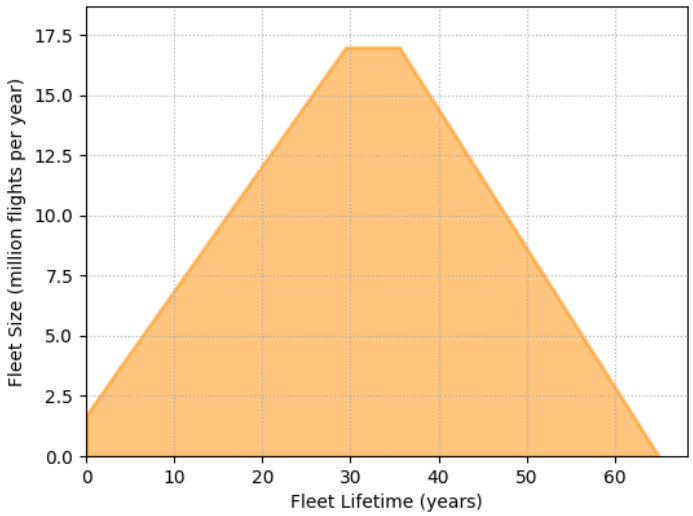

Figure 3.12: Fleet Definition in Number of Flights per Year.

4

Results

4.1. Baseline Aircraft

As the main results case, a medium range flight is considered to cover 4000km with a 16-ton payload. The aircraft design is fixed at the narrowbody baseline (Table 3.1) and the trajectory is optimised independently for direct operating cost (DOC) and average temperature response (ATR). The controls (alpha and T_{t4}) and selected states from the trajectories are shown in Figure 4.1. The DOC optimal trajectory is the baseline for comparison against all other 4000km optimisations. The most notable difference between the DOC and ATR cases is the altitude diversion between 1500km to 3000km of flight distance seen in the ATR optimal flight path. This avoids the contrail persistence region (CPR) and reduces the flight's climate impact by more than half (-54.8%; Table 4.1). Throughout the trajectory, the ATR optimal case maintains a lower cruise speed, maintaining a larger margin to the drag divergence velocity. This corresponds to a lower flight Mach number (Table 4.1) and minimises wave drag. The engine T_{t4} is also reduced, impacting both fuel burn and NO_x production. If NO_x effects were considered in the ATR objective, the optimal T_{t4} would likely be even lower (see Appendix 4.7).

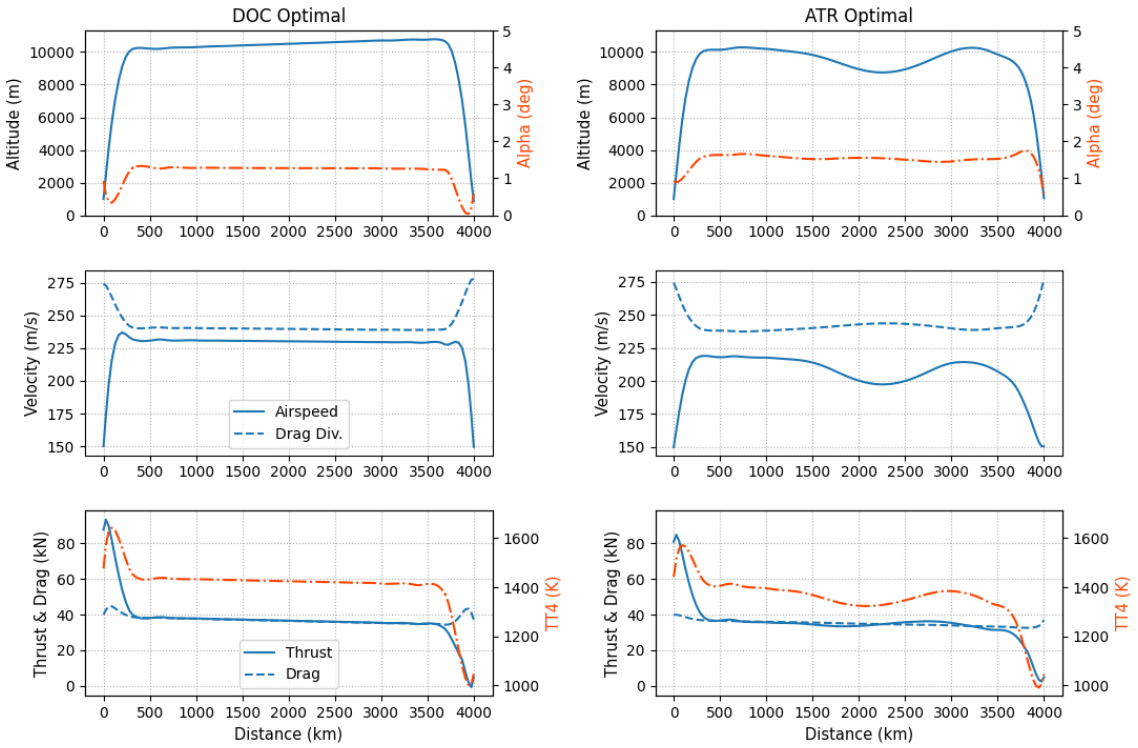

Figure 4.1: Optimised 4000km Trajectories for Baseline Aircraft with DOC (left) and ATR (right) Objectives.

Table 4.1 provides a comparison of indicative values for the objectives of DOC, ATR and fuel. This gives an indication of the potential for climate impact reduction with a relatively small increase in cost by avoiding contrail persistence regions. It also demonstrates the significance of non-CO_2 effects in the total climate impact, considering the differences between ATR- and fuel-optimal results.

Table 4.1: Comparison between DOC, ATR and Fuel-Optimal Trajectories.

	Min. DOC	**Min. ATR**	**Min. Fuel**	**Unit**
Fleet Lifetime Totals				
Operating Cost	**7.93**	8.29	8.11	10^{12} USD
ATR_{100}	17.6	**7.96**	18.5	mK
Fuel	5.74	5.65	**5.58**	10^{12} kg
Totals per Flight				
Time	04:53	05:25	05:15	hh:mm
Cruise Mach Number	0.774	0.730*	0.734	-
Avg.** Cruise T_{t4}	1430	1360	1400	K

*Cruise state for ATR case considered when unaffected by contrail persistence region (800km).
**Average taken over range 500-3500km.

To investigate the trade-off between DOC and ATR, the cost weighting ψ_c is varied from 1 to 0 (equivalently, the climate weighting ψ_a is varied from 0 to 1). Resulting flight paths for the baseline aircraft are shown in Figure 4.2. The cruise altitude in regions unaffected by contrail persistence (500-1000km) is relatively consistent between the trajectories. Cases with higher cost weightings have flight paths which pass closer to the contrail persistence region, trading climate optimality for cost optimality. However, even with relatively high cost weightings (up to 0.98), the CPR is mostly avoided (see Figure 4.4). *This demonstrates the cost-effectiveness of contrail avoidance to reduce climate impacts*.

Interestingly, the trajectory optimised for a very high cost weighting of 0.995 initially finds a route below the contrail region. Once the diversion from the cost-optimal cruise altitude becomes too costly (2000-2500km), the aircraft instead gains altitude again to minimise costs rather than climate impact.

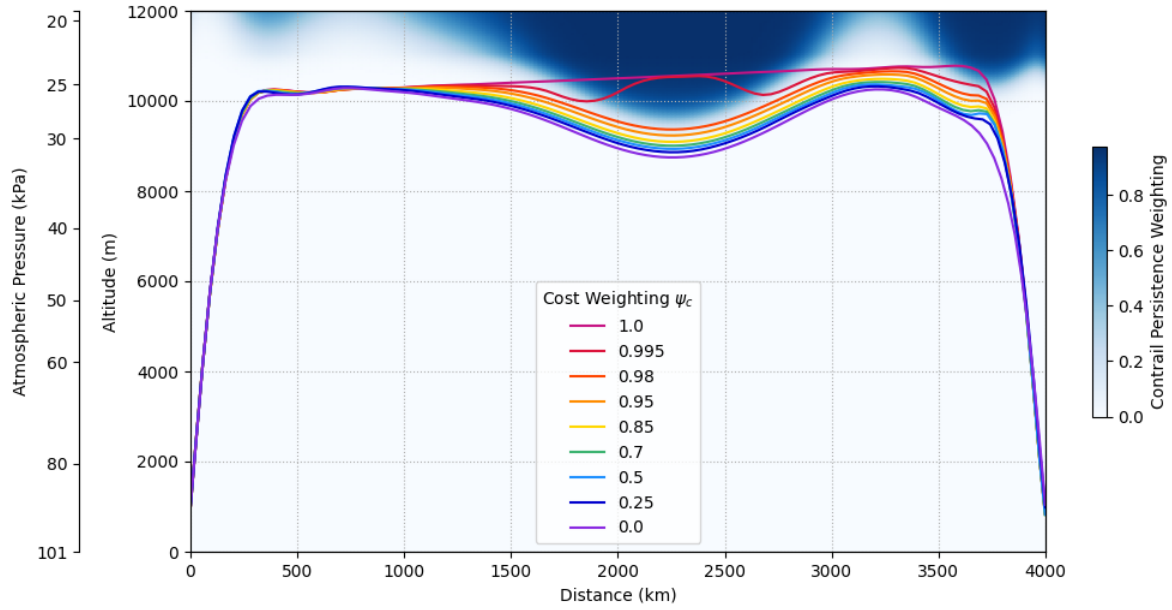

Figure 4.2: Optimised 4000km Trajectories for Baseline Aircraft with Varied Cost Weighting.

A cost breakdown in Figure 4.3 shows cost contributions associated with flight duration and fuel usage. As expected, the total cost increases for a reduced cost weighting, but the division between time and fuel-related costs reveals a more interesting trend. As the trajectory is optimised to consider ATR (i.e.

ψ_c is reduced from 1), the fuel cost initially increases while time cost decreases. This occurs as the aircraft flies further from the cost-optimal path but *increases* its flight velocity. At lower cost weightings, time-related costs rise rapidly and fuel costs decrease due to a lower flight velocity.

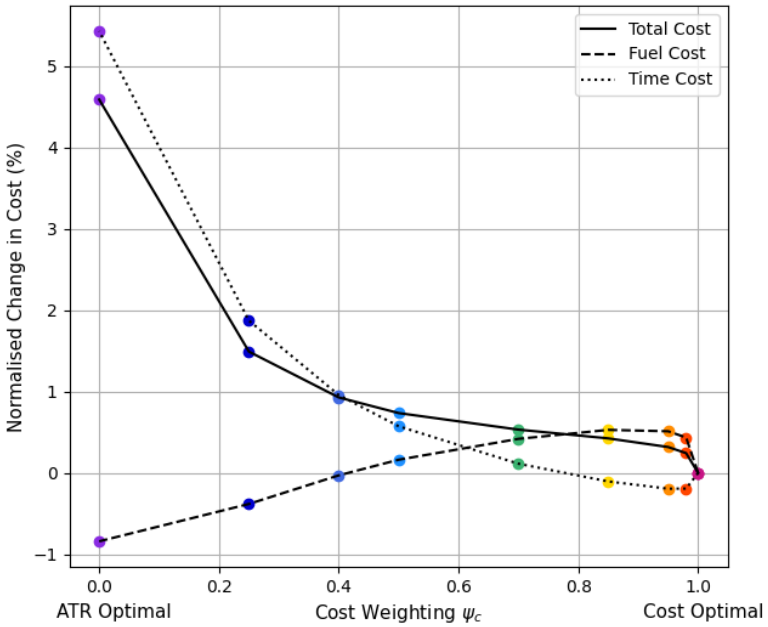

Figure 4.3: Relative Cost Breakdown for Varied Cost Weighting.

The division of emissions species contributions to the total ATR is given in Figure 4.4. All values are normalised by the total ATR of the cost optimal trajectory. The significance of contrail impacts and relative ease of minimising their effects is evident in the 44% ATR reduction associated with a cost weighting change from 1.0 to 0.98. This is substantiated by the DOC-ATR Pareto front in Figure 4.9. Carbon dioxide (CO_2) effects remain relatively stable across the range of cost weightings (as can be seen by the cost curve in Figure 4.3, the fuel burn decreases by less than 1%). Although nitrogen oxide (NO_x) effects are not directly included in the ATR objective, they decrease with the cost weighting. This appears as a side-effect of the reduced flight altitude and lower T_{t4} (see fig 4.1).

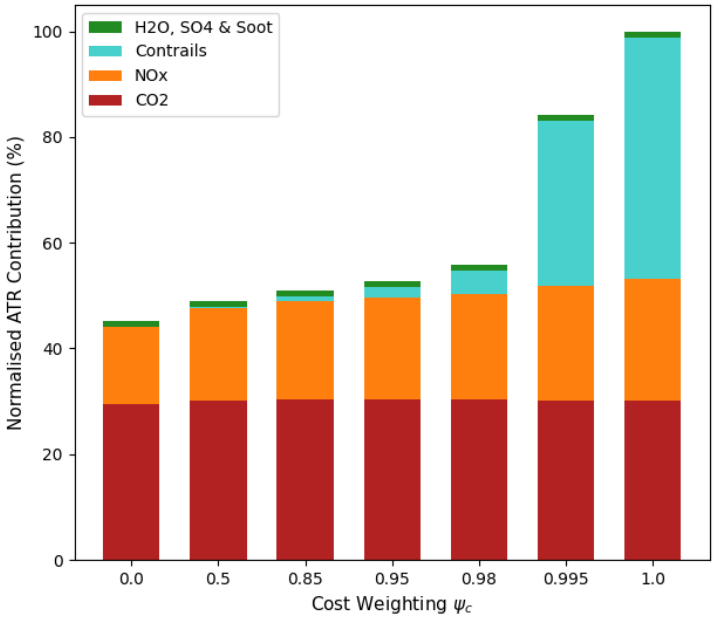

Figure 4.4: Normalised Emission Species Contributions to ATR for Different Cost Weightings.

Since the ATR is composed of short- and long-term effects, its evolution over time changes depending on the dominant emission species. Figure 4.5 illustrates the Earth's surface temperature response due to each emission species for the 100-year period over which the ATR is taken. It indicates that, although contrails and NO_x can be significantly reduced, their effects are relatively short-lived. On the other hand, CO_2 is a longer-impacting agent that will affect the climate for many decades after fleet retirement. This might lead to the impression that contrail and NO_x impact reduction is less valuable than CO_2 reduction. However, this should not detract from the potential warming that could be prevented by minimising impacts of the shorter-term agents. Furthermore, these insights might be even more worthwhile when considering hydrogen or sustainable aviation fuels which would directly eliminate or minimise CO_2 but not contrails or NO_x effects.

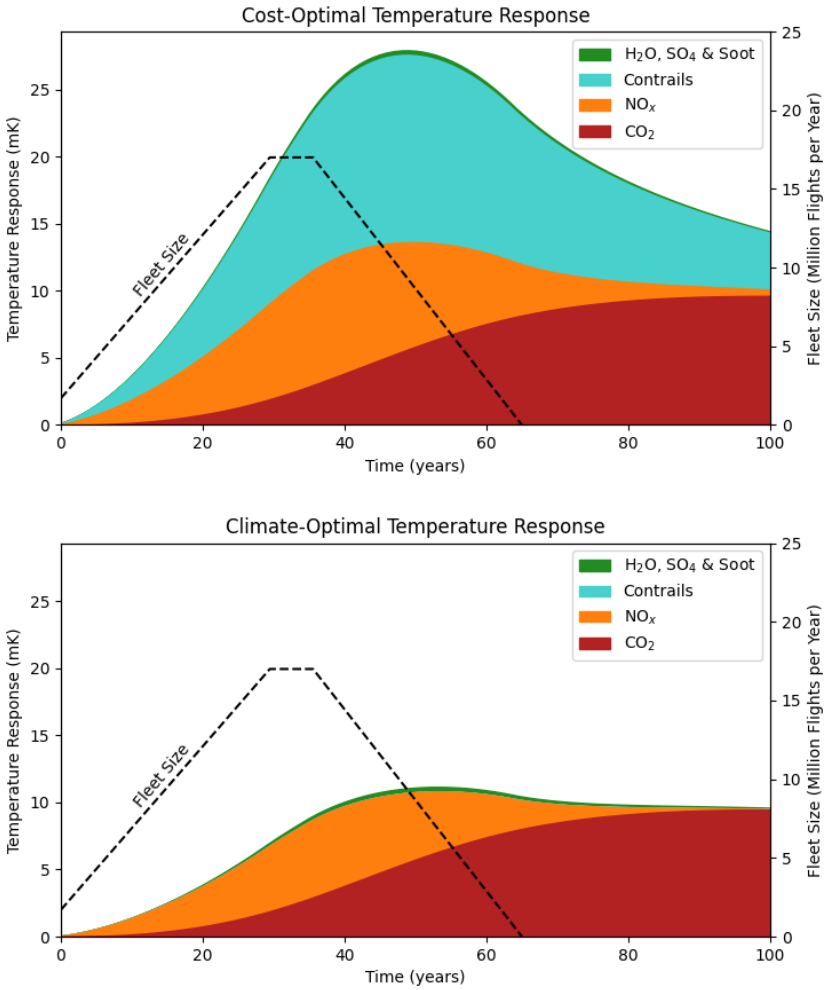

Figure 4.5: Temperature Response Compositing Over a 100-Year Period Due to Cost-Optimal and Climate Optimal Trajectories.

4.2. Optimised Aircraft

Using the aircraft parametrisation described in Section 3.2, wing aspect ratio, loading and quarter chord sweep are optimised alongside the trajectory. While the bypass ratio was also optimised, the technological upper bound of 11 was reached in every case and is therefore excluded from the results. This might differ with better engine parametrisation including pressure ratios and if NO_x was included in the ATR objective.

The flight paths in Figure 4.6 display one main difference from the baseline aircraft case; As the cost weighting decreases and priority is given to the ATR objective, cruise altitude decreases. This happens alongside a decrease in cruise Mach number, which is accompanied by a decreased wing sweep as

illustrated in Figure 4.7. A straight wing is optimal for cost weightings of 0.65 and below.

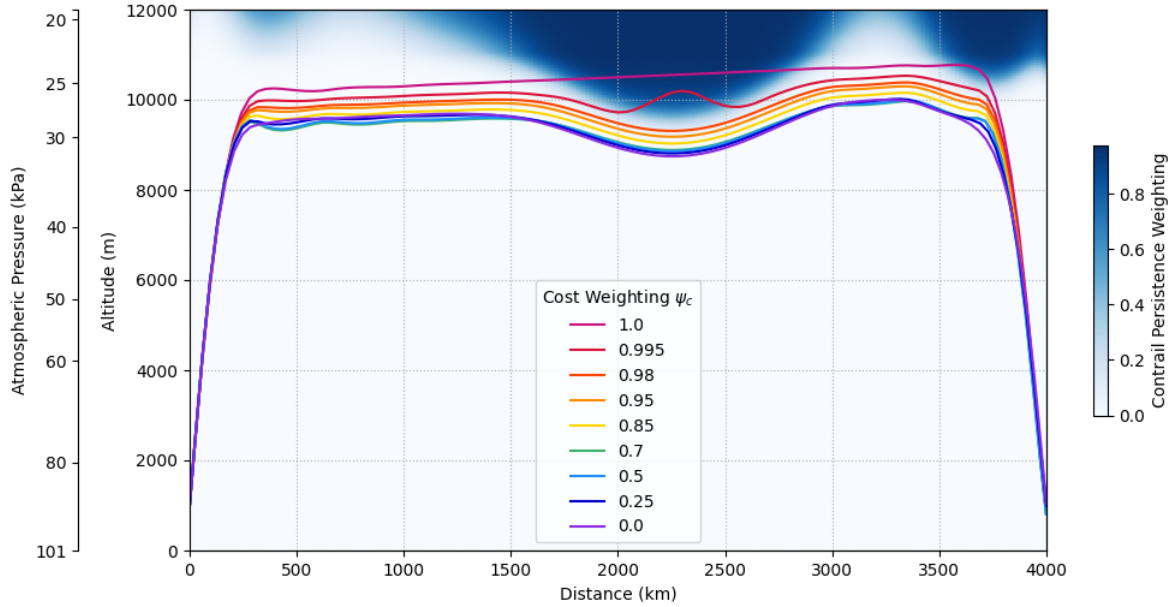

Figure 4.6: Optimised 4000km Trajectories for Optimal Aircraft with Varied Cost Weighting.

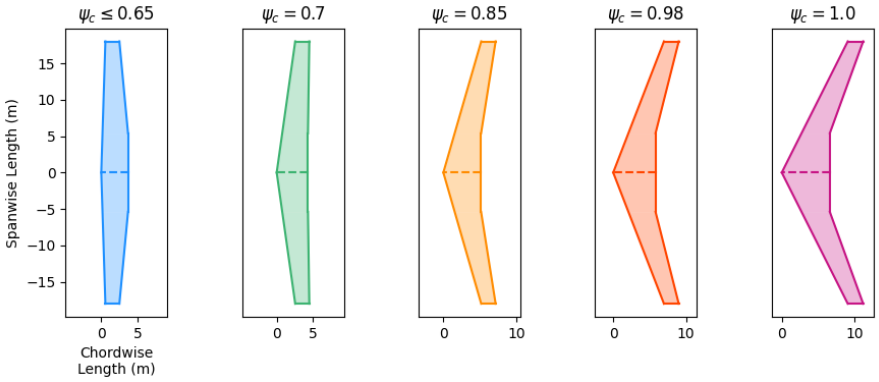

Figure 4.7: Optimised Wing Planforms for Varied Cost Weighting.

Figure 4.8 displays the wing sweep and aspect ratio relative to the cruise Mach number (outside of CPRs). It shows the effect of the cost weighting on the optimal cruise Mach number and how the design variables adjust simultaneously. With reduced Mach number, the optimal sweep decreases as it is becomes less critical in reducing wave drag. With lower sweep, the wing maximum lift coefficient rises and therefore a smaller wing and higher wing loading can be achieved.

In all cases the upper wingspan limit of 36m is reached, and the maximum takeoff weight is fixed. Therefore, the wing loading and aspect ratio become proportional, as shown in Equation 3.6. A higher wing loading is thus correlated to a higher wing aspect ratio.

$$\mathrm{AR} = \frac{b^2}{S_{\mathrm{ref}}} = \frac{b^2}{\mathrm{MTOW}} \cdot (W/S) \tag{4.1}$$

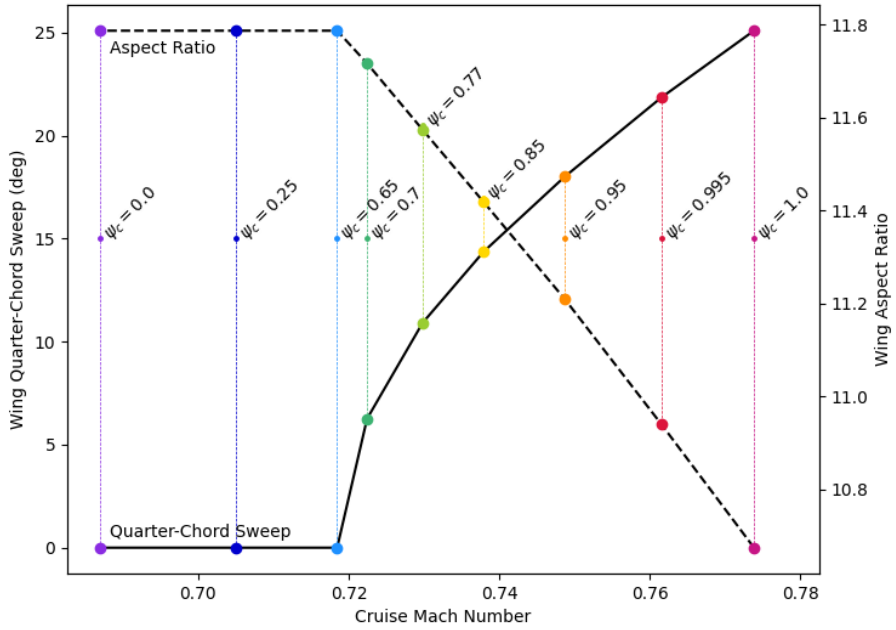

Figure 4.8: Relation Between Cruise Mach Number, Wing Sweep and Aspect Ratio with Varied Cost Weighting.

For cost weightings below 0.65, the wing becomes fixed with zero sweep (a straight wing). Instead, a further decrease in the cost weighting, and therefore Mach number, results in an *increased* cruise altitude. This is possible because the aircraft can avoid wave drag more easily at a lower cruise speed. It can therefore fly at a higher altitude where the speed of sound is lower.

4.3. Effect of Simultaneous Optimisation

The Pareto front in Figure 4.9 illustrates the trade-off between DOC and ATR, where values are normalised relative to the cost-optimal trajectory. This plot directly targets the research question, *demonstrating the cost effectiveness of climate mitigation through simultaneous optimisation*. The solid line indicates the baseline aircraft whose trajectory is optimised for different cost weightings. The front demonstrates the value of optimisation for different DOC-ATR weightings, as both extremes are undesirable - a cost-optimal trajectory has a large climate impact, whereas a fully ATR-optimal trajectory demands a 4.6% increase in operating costs.

Consider instead the trajectories for cost weightings between 0.5 and 0.98, where ATR is reduced by more than 40% and DOC rises by less than 1%. An attractive option is the cost weighting of 0.85, which provides a 49% reduction in ATR with only 0.42% increase in operating cost from the cost optimal solution. Interestingly, flight time in fact *decreases* very slightly from the cost-optimal case (-0.21%), but fuel burn increases by 1.0%. This prompts the question of how an optimised aircraft would perform for the same cost weighting.

The effect of simultaneous optimisation of the aircraft and its trajectory is shown by the shifted Pareto front (dashed line), illustrating an improvement in both DOC and ATR. Compare the new point corresponding to the cost weighting of 0.85. The ATR is now reduced by almost 56% from the baseline. Furthermore, the DOC has decreased negligibly (-0.21%) and fuel consumption decreases by 3.8%. Flight time, however, increases by 3.5%, equating to just more than 10 minutes over the five-hour flight. This improved Pareto point is enabled by the optimised wing planform in Figure 4.7, where sweep decreases from 25 to 14.4 degrees and aspect ratio increases by one point to 11.4.

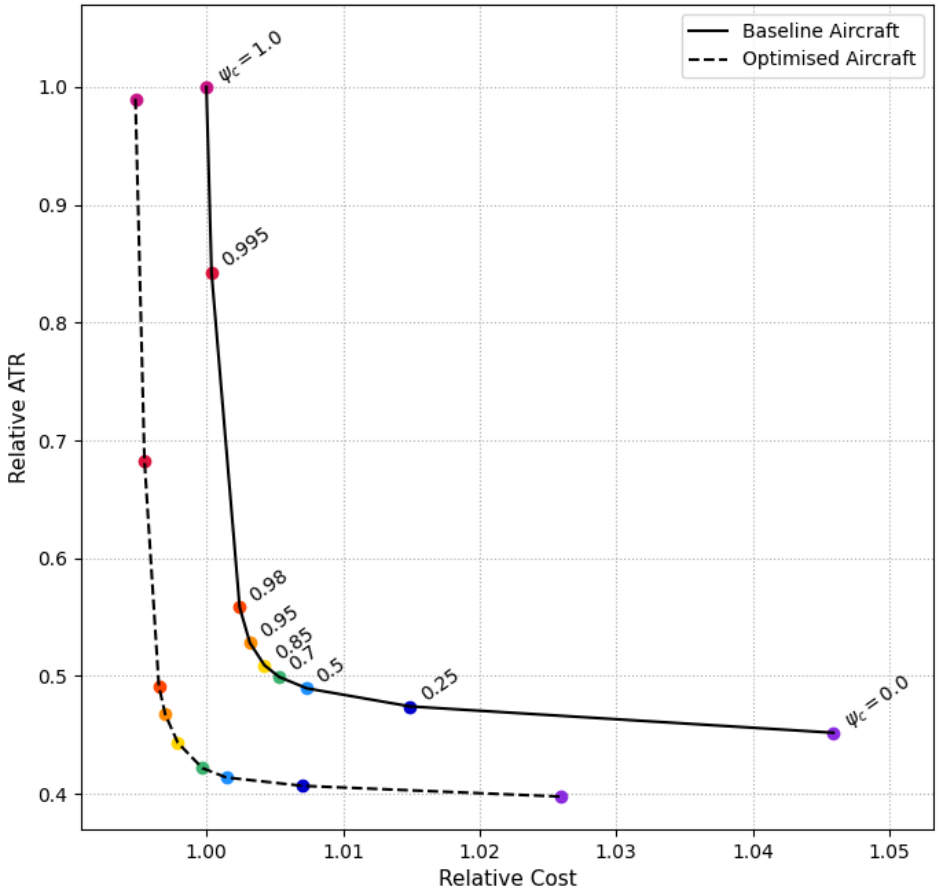

Figure 4.9: DOC-ATR Pareto Fronts for Baseline and Optimised Aircraft.

4.4. A Sensitivity Analysis on Aircraft Design Variables

Since the optimised aircraft designs for different cost weightings vary significantly from the baseline (see Figures 4.7 and 4.8), a sensitivity analysis is conducted to evaluate the effect of individually modified aircraft design variables. Wing aspect ratio, loading and quarter-chord sweep are varied independently for the case in which DOC and ATR are equally weighted in the objective ($\psi_c = \psi_a = 0.5$). Compared to the baseline, the optimal aircraft for this objective has an increased aspect ratio and wing loading, but decreased sweep. Therefore, the variables are independently modified with a 5% change in the direction of the optimal design to determine how they individually contribute to the resulting trajectory.

It is recognised that for a full sensitivity analysis, each variable should be independently varied without any other changes, including fixing the flight path. However, inconsistencies would result if only a design variable is changed and every other trajectory variable is fixed. For example, a change in wing loading might correspond to a different combination of cruise angle of attack, speed and altitude. Therefore, in each of the cases here, the trajectory is optimised for a given change to the baseline aircraft design at the fixed cost weighting of 0.5. Table 4.2 shows the effect of the changed design on the indicative trajectory values. The results are also overlaid on the Pareto front in Figure 4.10.

As might be expected, the increased aspect ratio and wing loading have similar effects, improving both fuel and climate optimality by 1-2%. The effect on flight time is small in comparison, and therefore the cost decreases due to reduced fuel consumption. The only notable differences between the two is that, compared to the aspect ratio change, increased wing loading leads to a slightly faster and less fuel-optimal flight (although still improved from the baseline).

Table 4.2: Sensitivity Analysis in Parametric Optimisation for DOC and ATR Objectives.

Change from Baseline	△ DOC	△ ATR	△ Fuel	△ Time	△ Early Cruise Alt.*
+ 5% Aspect Ratio	− 0.79%	− 1.34%	− 1.88%	+ 0.31%	+ 177 m
+ 5% Loading	− 0.76%	− 1.32%	− 1.24%	− 0.28%	+ 80 m
− 5% Sweep	+ 0.26%	− 0.56%	− 0.00%	+ 0.51%	− 35 m

*Early cruise taken at 800km flight range.

Wing sweep has a more complex effect. Most importantly, a straighter wing has greater susceptibility to wave-drag. The aircraft therefore flies slightly slower, as indicated by the flight time increase. Flight altitude is almost unchanged (Table 4.2), and therefore the change in ATR comes not from contrails but from lower NO_x emissions as a result of slower flight. The flight time increase raises the associated DOC. Each of the changes discussed is shown on broken-out sections of the Pareto front in Figure 4.10. The scale is fixed between the plots for ease of comparison.

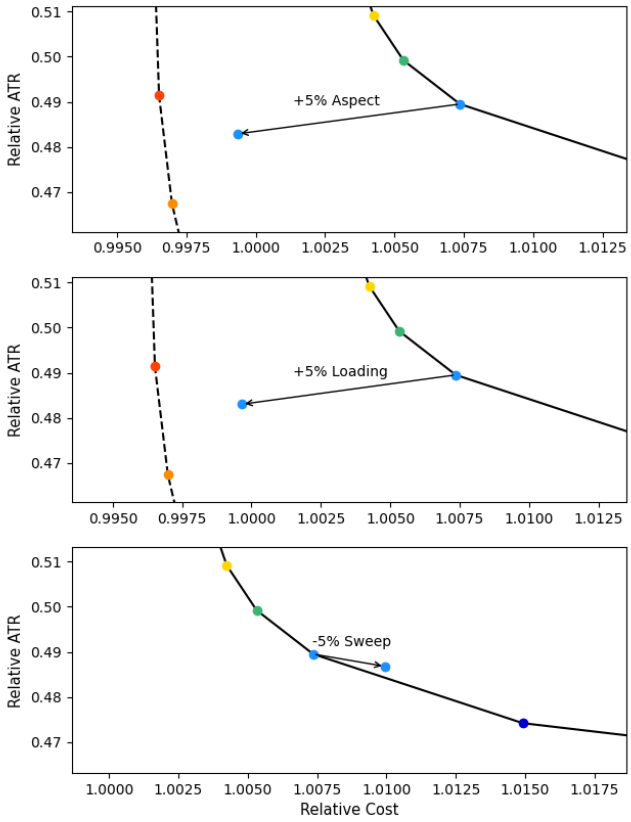

Figure 4.10: Sensitivity Analysis of Aircraft Parametric Optimisation on the DOC-ATR Pareto Front.

4.5. Effect of Alternative Atmospheric Conditions

Here, the effects of alternative atmospheric conditions are explored for the medium range route (4000km range, 16-ton payload). For this comparison, the aircraft design and trajectory are simultaneously optimised. Flight path results adjust to the new atmosphere, with trajectories optimised for cost-weightings of 0.98 and below effectively avoiding the new CPR in the early stages of the flight, shown in Figure 4.11. As before, a cost weighting of 0.995 generates interesting behaviour, as the aircraft avoids contrails only if it does not require too large a diversion from the cost-optimal path. This creates what appears as oscillatory behaviour in the early stages of the flight, but it is a response to the changing humidity. It seemingly contradicts the behaviour of flight paths for cost weightings of 0.98 and below, which effectively avoid the CPR.

Note in the ATR-optimal flight path ($\psi_c = 0$) the slightly flattened region at around 800km. This is a result of the Schmidt-Applemann Criterion (SAC) for contrail formation, which is based on the standard atmospheric temperature and pressure, and has a more sudden cut-off than the other persistence criteria (see Appendix Figure E.1). This is the only time the SAC restricts contrail formation in all the cases studied in this work.

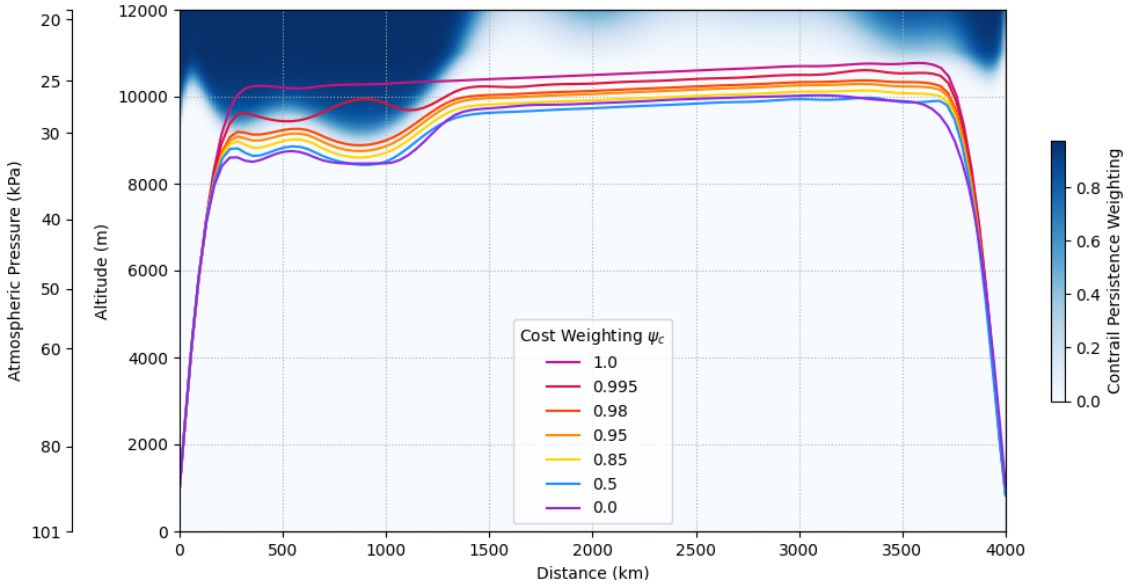

Figure 4.11: Optimised Trajectories in Alternative Atmospheric Conditions for Varied Cost Weightings.

Interestingly, the optimised aircraft variables for this second atmospheric case are almost identical to those from the main case for their respective cost weightings (see Figure 4.8). Optimised wing sweep values vary between the cases by around 0.1 degrees - differences which would be indistinguishable on the aforementioned plot. *This suggests that a fixed mdeium range aircraft design could be chosen based on a design cost weighting, assuming most flights take place in mid-latitudes*. Adding to this, the Pareto front for trajectories in the alternative atmosphere almost matches that for the first simultaneous optimisation case. For a cost weighting of 0.85, the optimised ATR varies by only 0.4% between the atmospheric cases. DOC variation is just 0.02%. Thus, the Pareto front for this case would appear unchanged to that in Figure 4.9.

Figure 4.12 shows the normalised contributions of emission species to the total ATR.

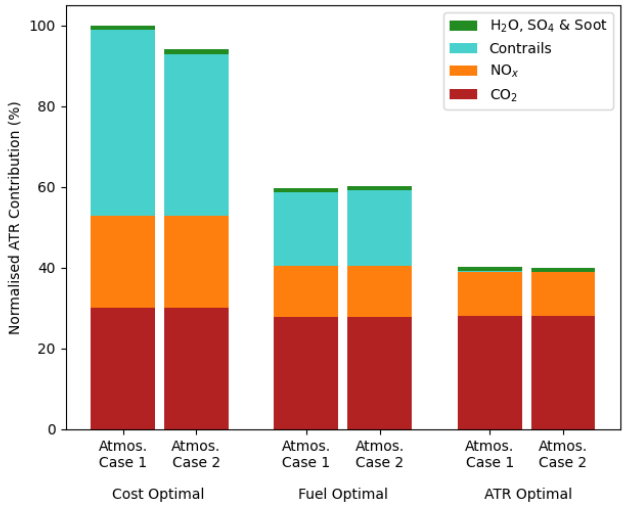

Figure 4.12: Normalised ATR Species Contributions for Different Atmospheric Conditions.

The only notable difference is the impact from contrails in the cost optimal cases, which are slightly reduced for atmospheric case 2 since the CPR covers less of the total flight distance. The similar results for an ATR optimal trajectory indicate that the location of the climate sensitive region has little effect on the optimal ATR, given that CPRs can be avoided. In higher-latitudes, ISSRs extend to lower altitudes and might be far more difficult to avoid in a cost effective manner.

4.6. Effect of Flight Range & Payload

The effect of range and payload is investigated through optimisation of a short range flight, covering 2000km with an 18-ton payload (see Payload-Range Figure 3.11). Although it is not possible to exactly compare the atmospheric humidity conditions from the baseline case due to its variation with range, a similar case is generated with using the same range-normalised polynomial spline as the baseline case (see Appendix F for humidity variation). The optimised flight paths for varied cost weightings are shown in Figure 4.13. The number of trajectory nodes is halved from the medium range case, using six instead of 12. This provides a smooth path with the equivalent physical node spacing in the trajectory time variable as the medium range case, leading to similar climb and descent path. It also reduces convergence time and prevents overfitting - in some cases with too many trajectory nodes, an oscillatory flight path would result.

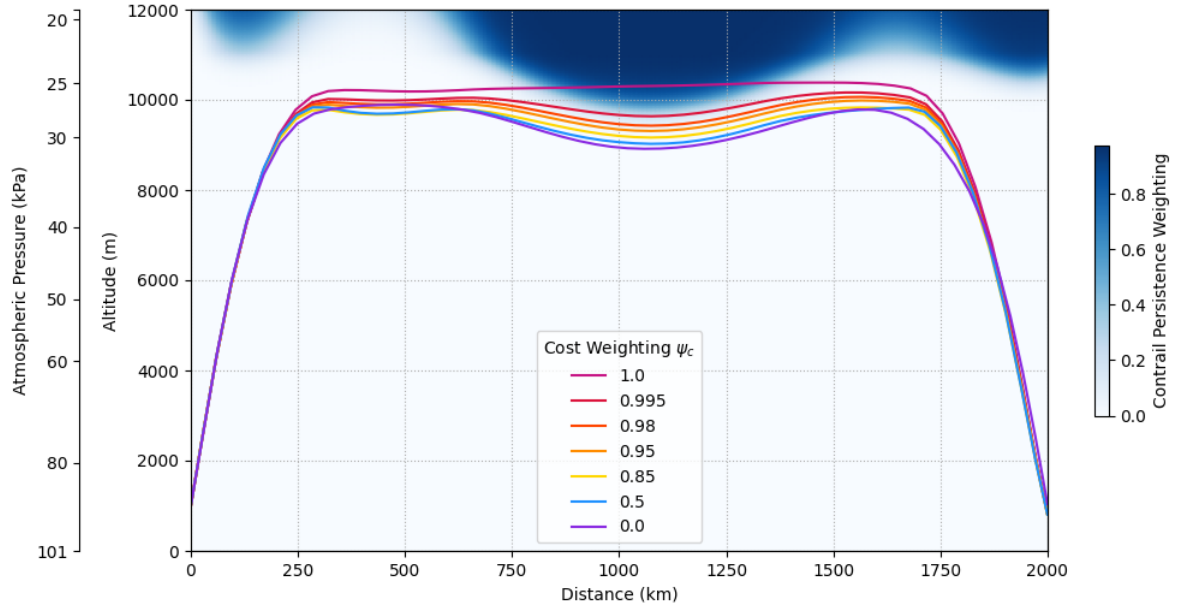

Figure 4.13: Short Range Optimal Flight Paths for Cost, Fuel and ATR Objectives.

The aircraft design variables are plotted against the cruise Mach number in Figure 4.14. For comparison, results from the medium range case are marked in light grey. The parameter variations match quite closely between cases, with differences most likely attributed to different aircraft mass in cruise - the short range aircraft burns less fuel and carries more payload, therefore having a higher average mass during cruise. This is also reflected by a slightly lower cruise altitude in the flight path plots.

It is worth noting in Figure 4.14 that the maximum sweep and minimum aspect ratio (corresponding to $\psi_c = 1.0$) are not as extreme as for the long range case. The aircraft designed for a cost-optimal short range trajectory corresponds to a cost weighting of around 0.98 in the medium range case (roughly 20-degree sweep and 11.1 aspect ratio). Additionally, the highest cost weighting at which a zero-sweep wing is optimal in the short range case is 0.78 compared to 0.65 in the medium range case. This suggests that lower sweep is a more optimal trade-off in shorter range aircraft and agrees with current aircraft design trends. Consider, for example, the straight wings of an ATR-72 and Bombardier Dash 8 optimised for ranges of around 2000 km, compared to the 25-degree sweep of the baseline narrowbody aircraft targeting up to 7000 km range.

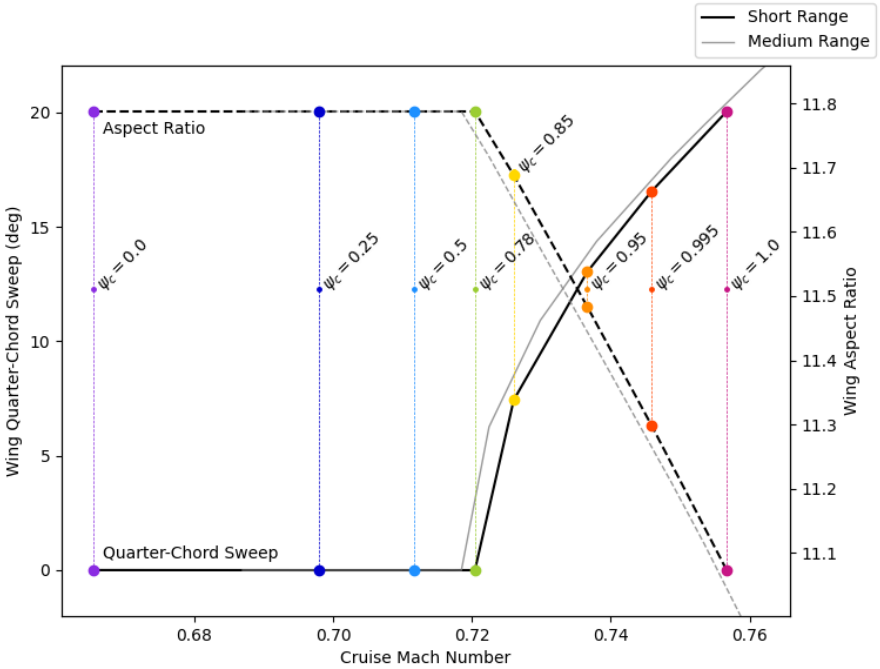

Figure 4.14: Normalised ATR Species Contributions for Different Flight Distances, Adjusted for Range and Payload.

A final comparison is highlighted in the ATR contributions from different emission species for DOC, fuel and ATR objectives in Figure 4.15. Both cases are normalised with respect to the baseline cost-optimal medium range case. Furthermore, the short range case is adjusted for range and payload, making results comparable as normalised ATR/(ton·km). This might be interpreted as an 'ATR efficiency' of the transport, and is seen to be consistently lower for the short range flight. A main contributor to this difference is the the reduced fuel requirement of short range flights, meaning a larger payload can be carried for the same emissions. This suggests that intermediate stop operations over longer routes could be beneficial for the climate.

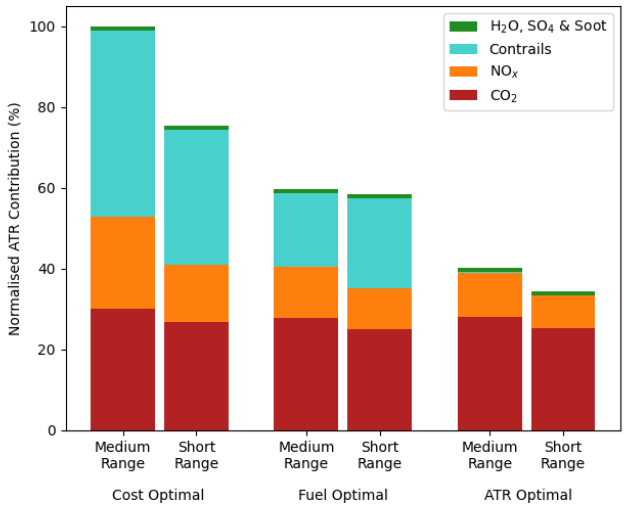

Figure 4.15: Normalised ATR Species Contributions for Different Flight Distances, Adjusted for Range and Payload.

4.7. Effect of Nitrogen Oxide in the ATR Objective

As mentioned in the objective function description (Sec. 3.3.3), the ATR objective does not include the effect of NO_x. In Figure 4.16, optimal trajectories are shown for an ATR objective including NO_x at cost weightings of 0 and 0.5. While not fully converged, the results offer insight into how the consideration of NO_x changes the optimal trajectory. A slightly faster climb and maximum T_{t4} is seen. This leads to high nitrogen oxide emissions at low altitudes, where its climate impact associated is neutral or even slightly negative, based on the methodology used. Cruise altitude is slightly reduced from previous ATR results which excluded NO_x. This allows a lower T_{t4} at cruise and limits NO_x emissions at high altitudes.

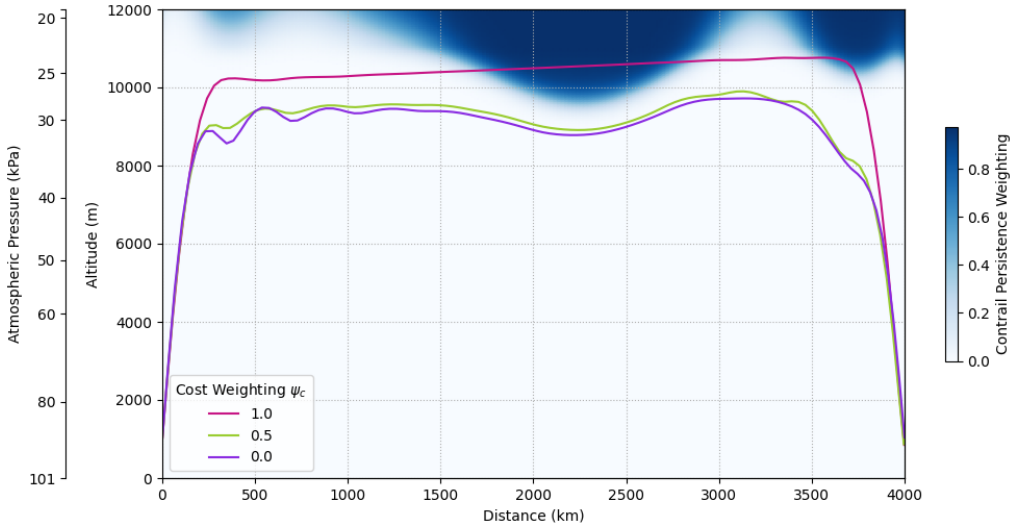

Figure 4.16: Optimised Trajectories for ATR Objective including NO_x.

Pareto fronts comparing results including and excluding NO_x from the ATR objective are shown in Figure 4.17. The front is slightly improved - consider the point for CI $=$ 0.5 for ATR including NO_x has a slightly lower ATR than the fully ATR optimal solution excluding NO_x. However, the reduction in total ATR is marginal and a fully ATR optimal trajectory considering NO_x incurs a significant increase in operating cost. This suggests that the benefits of considering NO_x in the trajectory objective might be limited. With better engine parametrisation to reduce NO_x emissions, such as modified pressure ratios and alternative combustor technology, the advantage might be more pronounced.

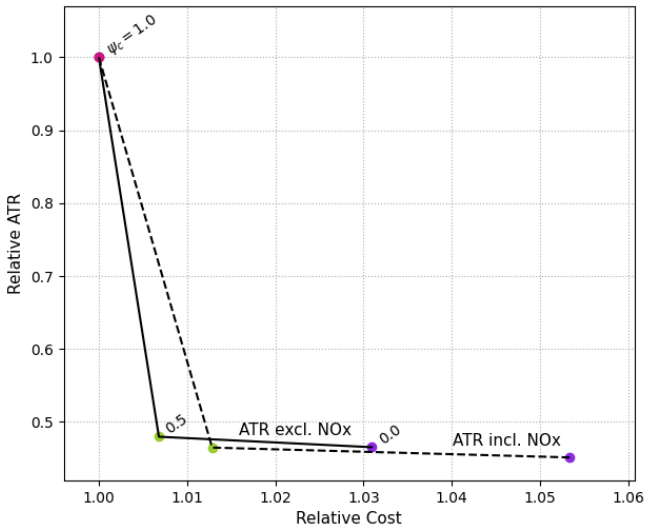

Figure 4.17: DOC-ATR Pareto Fronts for ATR Objective including and excluding NO_x.

5

Conclusions

The goal of this research has been to show that the climate impact of aviation can cost-effectively be reduced through simultaneous aircraft design and trajectory optimisation. This has been achieved using optimal control techniques to find medium range flight trajectories which minimise an objective composed of direct operating costs (DOC) and average temperature response (ATR). Results show that the ATR of a flight can be reduced more cost effectively when the trajectory is allowed full 2-dimensional freedom in the vertical plane when compared to a typical climb-cruise trajectory with optimised cruise altitude and Mach number.

Significant differences between the solutions for ATR-optimal and fuel-optimal trajectories demonstrate the importance of considering non-CO_2 climate effects, and how alternative flight path routing can be used to effectively reduce contrail impacts, even for a fixed baseline aircraft design. When a weighted objective of DOC and ATR is considered, the effect of contrail avoidance becomes even more clear. Only at a very high cost weighting of 0.995 and above does the optimised trajectory pass through contrail persistence regions, compromising climate impact for reduced operating cost. At slightly lower cost weightings (0.95 - 0.98), optimal trajectories are found in which contrail persistence is mostly avoided (approx. 90% contrail impact reduction), while flight time and time-related costs are also reduced from the cost optimal case. The overall cost increase is attributed to higher fuel burn. A highly favourable compromise is achieved with a cost weighting of 0.85, where the ATR is reduced by 49% and operating cost increases by just 0.42%.

When optimising the aircraft design simultaneously with the trajectory, the ATR can be reduced by a further 7% for a cost weighting of 0.85. Furthermore, the operating cost associated with this new trajectory and aircraft is comparable with the baseline case (-0.21%). The main compromise is a flight time increase of 3.5%, or 10 minutes over the 4000km route. Compared to the baseline narrowbody, the optimised aircraft has a wing sweep reduced to 14.4 degrees and an increased aspect ratio of 11.4. A significant improvement is seen when comparing the above case with an ATR optimised aircraft and cruise-climb trajectory studied by Proesmans and Vos [1], where the operating cost increased by around 1.8% for a 50% reduction in ATR. This is attributed to the flexibility of the trajectory optimisation, allowing a large portion of the flight to remain at a fuel-efficient altitude, only descending to avoid climate sensitive regions.

Alternative atmospheric humidity conditions, and therefore the locations of climate sensitive regions, appear to have little impact on the results for medium range flight, given that the atmosphere remains representative of mid-latitude conditions. The cost-climate Pareto front is almost unchanged between the two medium range atmospheric cases studied, with variations in DOC and ATR reaching just 0.02% and 0.4%, respectively, for a cost weighting of 0.85. The optimised aircraft designs are also almost independent of the atmospheric case, whereas they showed a much stronger dependency on the objective cost weighting. *This suggests that medium range aircraft could be designed based on a chosen weighting between cost and climate, and operate at a highly favourable DOC-ATR trade-off in different mid-latitude conditions.*

An aircraft optimised for shorter range flights tends to fly slower and hence have a lower wing sweep and higher aspect ratio than that for medium range flights. With lower fuel mass, aircraft can carry higher payloads over shorter flights and thereby have a lower fuel burn and ATR per ton·km. This indicates the benefits that might be achieved through intermediate stop operations for long distance transport. However, the impacts of this on cost and flight time would unlikely be justifiable. Instead, a single trajectory with a lower cost weighting might provide a more cost effective solution to reducing short-term climate impacts (contrails and NO_x).

Comparing DOC- and ATR-optimal trajectories, most of the climate impact reduction is attributed to the shorter-term impacts from contrails and NO_x, whereas longer-term impacts from CO_2 decrease by only 1.6%. It is therefore worthwhile considering whether climate impact mitigation through contrail avoidance is as valuable as that from minimising carbon dioxide emissions, which will affect the planet for many more decades. However, it is shown that a fuel-minimised flight (and therefore minimum CO_2) only results in a further 1.2% CO_2 emissions reduction. This indicates that methods other than aircraft design and trajectory optimisation will be required for larger carbon impact reductions. A promising solution might be to use sustainable aviation fuels or hydrogen rather than standard kerosene, as discussed in the introduction. A complementary scenario might see alternative fuels being used to minimise carbon emissions and trajectory optimisation targeting contrail avoidance.

While the impacts of nitrogen oxides are not included in the ATR objective, it appears that the loss in climate optimality due to this assumption is not large. Results indicate that a trajectory with minimised NO_x effects would result in undesirably large cost and flight time compromises for airlines and passengers. Although a fully optimal point was not reached for an ATR objective including NO_x, results suggest that a steeper climb profile which produces high levels of NO_x at low altitude would reduce the ATR of a flight. This, however, would have an undesirable impact on air quality at low altitudes and may affect human, animal and plant health. Furthermore, optimising trajectories for ATR using this parametrisation technique while including NO_x produces severe flight path oscillations. This is likely because NO_x emissions *can* be favourable at low altitudes but unfavourable at high altitudes, thus the thrust and altitude oscillate to minimise the ATR. Proper optimisation of the trajectory and aircraft for NO_x impacts would require better engine parametrisation and careful constraint of the allowable flight path to eliminate oscillations. Furthermore, better study and modelling of the climate impacts of NO_x, including how it affects life in the biosphere and the longer-term climate impacts of this, might conclude that NO_x is more damaging in the lower atmosphere than predicted by the models used in this study. In that case, minimising NO_x emissions should be targeted in all cases.

Finally, it is worth considering the convergence behaviour of the engine bypass ratio. Typically, high bypass engines have high propulsive efficiency. However, lower bypass ratio engines with a hotter exhaust are less likely to result in contrails due to the condensation characteristics of the hot exhaust mixed with ambient air (see the description the Schmidt-Appelman Criterion and contrail persistence in Section 3.4.2). It therefore seems likely that the optimal engine bypass ratio for a minimum ATR trajectory might be lower than the baseline. However, in all cases the optimised engine bypass ratio reaches the upper bound of 11. Contrails are instead avoided by routing below persistence regions. This indicates that the benefit of a high bypass ratio engine in terms of fuel economy is great enough to offset the additional fuel burn from flight path rerouting to avoid contrails.

6

Recommendations and Future Work

6.1. Trajectory

Dymos can be used to optimise a parametric design considering its operation on a number of trajectories. This feature would be useful to analyse and optimise an aircraft design over several routes that it might be expected to cover. For example, several routes of different ranges and atmospheric conditions could be defined and optimal trajectories developed, with an aircraft design that is optimised considering all of the routes.

6.2. Aircraft Parametrisation

6.2.1. Wing Parametrisation

The aircraft design module used in this work is simplified. Improvement could be offered in the consideration for how design variables affect the aircraft structural weight, with particular reference to the wing sweep and aspect ratio. Additionally, since the landing approach constraint was highly impactful in these results, the effect of high lift devices could be better studied to gain a better understanding of how sweep impacts the maximum lift coefficient.

6.2.2. Engine Model

The engine parametrisation was simplified to include only the bypass ratio. In simultaneous optimisations, this quickly converged to one of the bounds. Realistically, the bypass should be optimised alongside the pressure ratios of the low- and high-pressure compressors (LPC & HPC). This is because the overall pressure ratio affects the power available to drive the fan, and therefore has an impact on the optimal bypass ratio. Inclusion of the LPC and HPC pressure ratios would also be interesting as these impact NO_x production.

6.3. Climate Model

6.3.1. Humidity Model

An improved humidity model, possibly including a forecast or historical 2D/3D data would make for a more realistic trajectory optimisation based on contrail formation and NO_x impacts. As mentioned in the background to optimal trajectories, there can be conditions in which a passing aircraft generates a cooling effect. These can be caused by the phenomenon know as distrails, where an aircraft flying through cloud causes condensed droplets to freeze and fall to warmer altitudes. Reduced cloudiness allows more terrestrial radiation to escape the atmosphere, thus having a cooling effect. An improved climate model could account for this by modelling cloudy regions which are sensitive to distrails, which might allow further reduction to the climate impact associated with a flight.

6.3.2. Effect of Nitrogen Oxides

Complexities arise from the combination of ATR-positive ozone impacts and ATR-negative methane impacts, the combined effect of which depends on emission altitude. At low altitudes, NO_x emissions are associated with a neutral or even negative ATR (cooling) impact, whereas positive ATR results

from NO_x emissions at typical cruise altitudes. Since NO_x emissions are closely related to the throttle control T_{t4}, a high throttle level is preferred at low altitude, whereas a low throttle level helps to reduce NO_x impacts at high altitude. This results in a highly oscillatory trajectory and unstable parametric optimisation. Work to better constrain the trajectory or manage the effects of NO_x in the objective could lead to further ATR improvements.

6.4. An Observation on Initialisation within a Simultaneous Optimisation Routine

As is typical for most optimisation problems, the initial conditions have a large impact on the progress and result of a simultaneous trajectory and design optimisation. It was discovered during some optimisations that the parametrised wing sweep had no effect on the objective function (e.g. cost, fuel or ATR). This was due to the initialised trajectory imposing only low subsonic flight conditions in which wave drag (present only in high subsonic and transonic conditions) played no role in the total aircraft drag. Usually, wing sweep is used to minimise the effects of drag divergence during high subsonic cruise. Thus, early on in the optimisation, the optimiser disabled its gradient search for the impact of wing sweep on the drag (and therefore the objective function), leading to a solution with a fixed zero-sweep wing. Initialising the trajectory using a previously optimised flight path including regions of high subsonic flight prevents this gradient disabling from occurring and leads to a more optimal solution which fully considers the effect of sweep.

References

[1] Pieter-Jan Proesmans and Roelof Vos. “Airplane Design Optimization for Minimal Global Warming Impact”. In: *Journal of Aircraft* (22nd June 2022), pp. 1–19. DOI: 10.2514/1.C036529.

[2] Sola Zheng and Dan Rutherford. *Fuel burn of new commercial jet aircraft: 1960 to 2019*. 2020, Washingtion, DC. URL: https://theicct.org/sites/default/files/publications/Aircraft-fuel-burn-trends-sept2020.pdf.

[3] D. S. Lee et al. “The contribution of global aviation to anthropogenic climate forcing for 2000 to 2018”. In: *Atmospheric Environment* 244 (1st Jan. 2021), p. 117834. DOI: 10.1016/j.atmosenv.2020.117834.

[4] D. S. Lee et al. “Transport impacts on atmosphere and climate: Aviation”. In: *Atmospheric Environment*. Transport Impacts on Atmosphere and Climate: The ATTICA Assessment Report 44.37 (1st Dec. 2010), pp. 4678–4734. DOI: 10.1016/j.atmosenv.2009.06.005.

[5] Guy P. Brasseur et al. “Impact of Aviation on Climate: FAA’s Aviation Climate Change Research Initiative (ACCRI) Phase II”. In: *Bulletin of the American Meteorological Society* 97.4 (1st Apr. 2016), pp. 561–583. DOI: 10.1175/BAMS-D-13-00089.1.

[6] Airbus S.A.S. *Cities, Airports & Aircraft: Global Market Forecast*. 5th ed. Blagnac Cedex, 2019. URL: https://www.airbus.com/sites/g/files/jlcbta136/files/2021-07/Airbus-GMF2019-presentation-Christian-Scherer.pdf.

[7] Ahmed W.A. Hammad et al. “Mathematical optimization in enhancing the sustainability of aircraft trajectory: A review”. In: *International Journal of Sustainable Transportation* 14.6 (2nd June 2020). Publisher: Taylor & Francis, pp. 413–436. DOI: 10.1080/15568318.2019.1570403.

[8] Ulrike Burkhardt and Bernd Kärcher. “Global radiative forcing from contrail cirrus”. In: *Nature Climate Change* 1.1 (Apr. 2011). Publisher: Nature Publishing Group, pp. 54–58. DOI: 10.1038/nclimate1068.

[9] Benjamin Lührs et al. “Cost-Benefit Assessment of 2D and 3D Climate And Weather Optimized Trajectories”. In: *16th AIAA Aviation Technology, Integration, and Operations Conference*. Vol. 16. AIAA AVIATION Forum. 10th June 2016. DOI: 10.2514/6.2016-3758.

[10] David I. Barton, Cesare A. Hall and Matthew K. Oldfield. “Design of a Hydrogen Aircraft for Zero Persistent Contrails”. In: *Aerospace* 10.8 (Aug. 2023). Number: 8 Publisher: Multidisciplinary Digital Publishing Institute, p. 688. DOI: 10.3390/aerospace10080688. URL: https://www.mdpi.com/2226-4310/10/8/688 (visited on 19/04/2024).

[11] Liam Megill. “Analysis of Climate Metrics for Aviation”. PhD thesis. Delft, The Netherlands: Delft University of Technology, 2022. 102 pp. URL: https://repository.tudelft.nl/islandora/object/uuid%3A9e84ee4d-af69-4550-8938-2ccf4caccb8c.

[12] Design Science and Technology Sub Group. “Mitigating the environmental impact of aviation: Opportunities and priorities”. In: *The Aeronautical Journal* 109.1099 (Sept. 2005), pp. 361–416. DOI: 10.1017/S0001924000000841.

[13] G. Lammel and H. Graßl. “Greenhouse effect of NOX”. In: *Environmental Science and Pollution Research International* 2.1 (July 1995), pp. 40–45. DOI: 10.1007/BF02987512.

[14] EASA. *How sustainable are SAF?* EASA Eco. 2023. URL: https://www.easa.europa.eu/eco/eaer/topics/sustainable-aviation-fuels/how-sustainable-are-saf.

[15] Volker Grewe et al. “Mitigating the Climate Impact from Aviation: Achievements and Results of the DLR WeCare Project”. In: *Aerospace* 4.3 (Sept. 2017). Publisher: Multidisciplinary Digital Publishing Institute, p. 34. DOI: 10.3390/aerospace4030034.

[16] Airbus. *Imagine travelling in this blended wing body aircraft*. 10th Sept. 2021. URL: https://www.airbus.com/en/newsroom/stories/2020-11-imagine-travelling-in-this-blended-wing-body-aircraft.

[17] G. J. de Zoeten, Carmine Varriale and Roelof Vos. “Flight Performance Evaluation of the Flying-V”. In: *AIAA AVIATION 2023 Forum*. 2023. DOI: 10.2514/6.2023-3484.

[18] Jacopo Prisco. *JetZero: Groundbreaking ‘blended-wing’ demonstrator plane cleared to fly*. CNN. 4th Apr. 2024. URL: https://www.cnn.com/travel/jetzero-pathfinder-subscale-demonstrator/index.html.

[19] Nicolas E. Antoine and Ilan M. Kroo. “Framework for Aircraft Conceptual Design and Environmental Performance Studies”. In: *AIAA Journal* 43.10 (Oct. 2005), pp. 2100–2109. DOI: 10.2514/1.13017.

[20] Katrin Dahlmann et al. “Climate-Compatible Air Transport System—Climate Impact Mitigation Potential for Actual and Future Aircraft”. In: *Aerospace* 3.4 (Dec. 2016). Publisher: Multidisciplinary Digital Publishing Institute, p. 38. DOI: 10.3390/aerospace3040038.

[21] Emily Schwartz and Ilan Kroo. “Aircraft Design for Reduced Climate Impact”. In: *49th AIAA Aerospace Sciences Meeting including the New Horizons Forum and Aerospace Exposition*. Vol. 49. Aerospace Sciences Meetings. Orlando, Florida: American Institute of Aeronautics and Astronautics, 4th Jan. 2011. DOI: 10.2514/6.2011-265.

[22] O. Boucher et al. “Comparison of Actual and Time-Optimized Flight Trajectories in the Context of the In-Service Aircraft for a Global Observing System (IAGOS) Programme”. In: *Aerospace* 10.9 (2023). DOI: 10.3390/aerospace10090744.

[23] Banavar Sridhar, Hok K. Ng and Neil Y. Chen. “Aircraft Trajectory Optimization and Contrails Avoidance in the Presence of Winds”. In: *Journal of Guidance, Control, and Dynamics* 34.5 (Sept. 2011), pp. 1577–1584. DOI: 10.2514/1.53378.

[24] Judith Rosenow, Martin Lindner and Joachim Scheiderer. “Advanced Flight Planning and the Benefit of In-Flight Aircraft Trajectory Optimization”. In: *Sustainability* 13.3 (Jan. 2021). Publisher: Multidisciplinary Digital Publishing Institute, p. 1383. DOI: 10.3390/su13031383.

[25] M. Niklaß et al. “Are climate restricted areas a viable interim climate mitigation option over the north atlantic?” In: 16th AIAA Aviation Technology, Integration, and Operations Conference. 2016. ISBN: 978-1-62410-440-4.

[26] A. Simorgh et al. “Robust 4D climate-optimal flight planning in structured airspace using parallelized simulation on GPUs: ROOST V1.0”. In: *Geoscientific Model Development* 16.13 (2023), pp. 3723–3748. DOI: 10.5194/gmd-16-3723-2023.

[27] James T. Allison and Daniel R. Herber. “Special Section on Multidisciplinary Design Optimization: Multidisciplinary Design Optimization of Dynamic Engineering Systems”. In: *AIAA Journal* 52.4 (Apr. 2014), pp. 691–710. DOI: 10.2514/1.J052182.

[28] Shugo Kaneko and Joaquim R. Martins. “MDO Formulations for Simultaneous Design and Trajectory Optimization”. In: *AIAA SCITECH 2024 Forum*. 4th Jan. 2024. DOI: 10.2514/6.2024-2231.

[29] John T. Hwang, John P. Jasa and Joaquim R. R. A. Martins. “High-Fidelity Design-Allocation Optimization of a Commercial Aircraft Maximizing Airline Profit”. In: *Journal of Aircraft* 56.3 (May 2019). Publisher: American Institute of Aeronautics and Astronautics, pp. 1164–1178. DOI: 10.2514/1.C035082.

[30] Michael Husemann, Katharina Schäfer and Eike Stumpf. “Flexibility within flight operations as an evaluation criterion for preliminary aircraft design”. In: *Journal of Air Transport Management* 71 (1st Aug. 2018), pp. 201–214. DOI: 10.1016/j.jairtraman.2018.04.007.

[31] Benjamin Yan, Peter Jansen and Ruben Perez. “Multidisciplinary Design Optimization of Airframe and Trajectory Considering Cost, Noise, and Fuel Burn”. In: *AIAA (ATIO)*. Indianapolis, Indiana: American Institute of Aeronautics and Astronautics, 17th Sept. 2012. DOI: 10.2514/6.2012-5494.

[32] Victor M. Becerra. “Optimal control”. In: *Scholarpedia* 3.1 (18th Jan. 2008), p. 5354. DOI: 10.4249/scholarpedia.5354.

[33] K.K.H. NG. “Emission-aware adjustable robust flight path planning with respect to fuel and contrail cost”. In: *Transportmetrica B* 11.1 (2023), pp. 24–68. DOI: 10.1080/21680566.2022.2036651.

[34] Y. Xu et al. “Machine-Learning-Assisted Optimization of Aircraft Trajectories Under Realistic Constraints”. In: *Journal of Guidance, Control, and Dynamics* 46.9 (2023), pp. 1814–1825. DOI: 10.2514/1.G007038.

[35] Y. Lim, A. Gardi and R. Sabatini. “Contrail Modelling for 4D Trajectory Optimisation”. In: *Sustainable Aviation Technology and Operations: Research and Innovation Perspectives*. 2023, pp. 475–497. DOI: 10.1002/9781118932599.ch19.

[36] Anil V. Rao. “Trajectory Optimization”. In: *Encyclopedia of Aerospace Engineering* (2010). DOI: 10.1002/9780470686652.eae502.

[37] Robert Falck et al. “dymos: A Python package for optimal control of multidisciplinary systems”. In: *The Open Journal* 6.59 (31st Mar. 2021), p. 2809. DOI: 10.21105/joss.02809.

[38] Matthew Kelly. *Introduction to Trajectory Optimization*. 2nd May 2016. URL: https://www.youtube.com/watch?v=wlkRYMVUZTs.

[39] Divya Garg et al. “An overview of three pseudospectral methods for the numerical solution of optimal control problems”. Oct. 2017. URL: https://hal.science/hal-01615132.

[40] J. Rosenow et al. “Validation of a Contrail Life-Cycle Model in Central Europe”. In: *Sustainability (Switzerland)* 15.11 (2023). DOI: 10.3390/su15118669.

[41] Emily Schwartz Dallara, Ilan M. Kroo and Ian A. Waitz. “Metric for Comparing Lifetime average Climate Impact of Aircraft”. In: *AIAA Journal* 49.8 (Aug. 2011), pp. 1600–1613. DOI: 10.2514/1.J050763.

[42] Christine Frömming et al. “Climate cost functions as a basis for climate optimized flight trajectories”. In: *Proceedings of the 10th USA/Europe Air Traffic Management Research and Development Seminar, ATM 2013* (1st Jan. 2013). URL: https://www.researchgate.net/publication/289622007_Climate_cost_functions_as_a_basis_for_climate_optimized_flight_trajectories.

[43] Banavar Sridhar et al. “Design of aircraft trajectories based on trade-offs between emission sources”. In: *Proceedings of the 9th USA/Europe Air Traffic Management Research and Development Seminar, ATM 2011* (1st Jan. 2011), pp. 54–63. URL: https://elib.dlr.de/95127/1/ATM2011_Sridhar.pdf.

[44] Andrew B. Lambe and Joaquim R. R. A. Martins. “Extensions to the design structure matrix for the description of multidisciplinary design, analysis, and optimization processes”. In: *Structural and Multidisciplinary Optimization* 46.2 (Aug. 2012), pp. 273–284. DOI: 10.1007/s00158-012-0763-y.

[45] Airbus S.A.S. Customer Services. *Airbus A320 Aircraft Characteristics Airport and Maintenance Planning*. 2022. URL: https://www.airbus.com/sites/g/files/jlcbta136/files/2022-02/Airbus-techdata-AC_A320_0322.pdf.

[46] Ed Obert. *Aerodynamic Design of Transport Aircraft*. IOS Press, 2009.

[47] Isaac Held. *Relative humidity in “cloud resolving” models – Geophysical Fluid Dynamics Laboratory*. 2012. URL: https://www.gfdl.noaa.gov/blog_held/26-relative-humidity-in-cloud-resolving-models/.

[48] Junzi Sun, Joost Ellerbroek and Jacco Hoekstra. *OpenAP: An open-source aircraft performance model for air transportation studies and simulations*. 15th May 2020.

[49] Gabriel Pinho Chiozzotto. “Improving aircraft conceptual design with methods for wing loads, aeroelasticity and mass estimation”. thesis. Technische Universität Berlin, 2019. 314 pp. URL: https://elib.dlr.de/127503/.

[50] Jack D. Mattingly, William H. Heiser and David T. Pratt. *Aircraft Engine Design, Second Edition*. Reston, Virginia: American Institute of Aeronautics and Astronautics, 2002. URL: https://doi.org/10.2514/4.861444.

[51] Emily Schwartz Dallara. “Aircraft Design for Reduced Climate Impact”. PhD thesis. Stanford, UK: Stanford University, 2011. URL: http://purl.stanford.edu/yf499mg3300.

[52] Airbus. “Getting to grips with the cost index”. In: (1998). URL: https://ansperformance.eu/library/airbus-cost-index.pdf.

[53] Robert Sausen and Ulrich Schumann. “Estimates of the Climate Response to Aircraft CO2 and NOxEmissions Scenarios”. In: *Climatic Change* 44.1 (1st Jan. 2000), pp. 27–58. DOI: 10.1023/A:1005579306109. URL: https://doi.org/10.1023/A:1005579306109.

[54] D Sonntag. “Important new values of the physical constants of 1986, vapour pressure formulations based on the ITS-90, and psychrometer formulae”. In: 40.5 (1990). Place: Berlin Publisher: Akademie-Verlag, pp. 340–344. ISSN: 0084-5361.

[55] Michael Ponater et al. “Potential of the cryoplane technology to reduce aircraft climate impact: A state-of-the-art assessment”. In: *Atmospheric Environment* 40.36 (1st Nov. 2006), pp. 6928–6944. DOI: 10.1016/j.atmosenv.2006.06.036.

[56] Intergovernmental Panel on Climate Change. *Climate Change 2007: The Physical Science Basis, Contribution of Working Group I to the Fourth Assessment Report of the Intergovernmental Panel on Climate Change*. Chapter 2. Cambridge, England, U.K.: Cambridge University Press, 2007, pp. 129–234.

A

Full Extended Design Structure Matrix

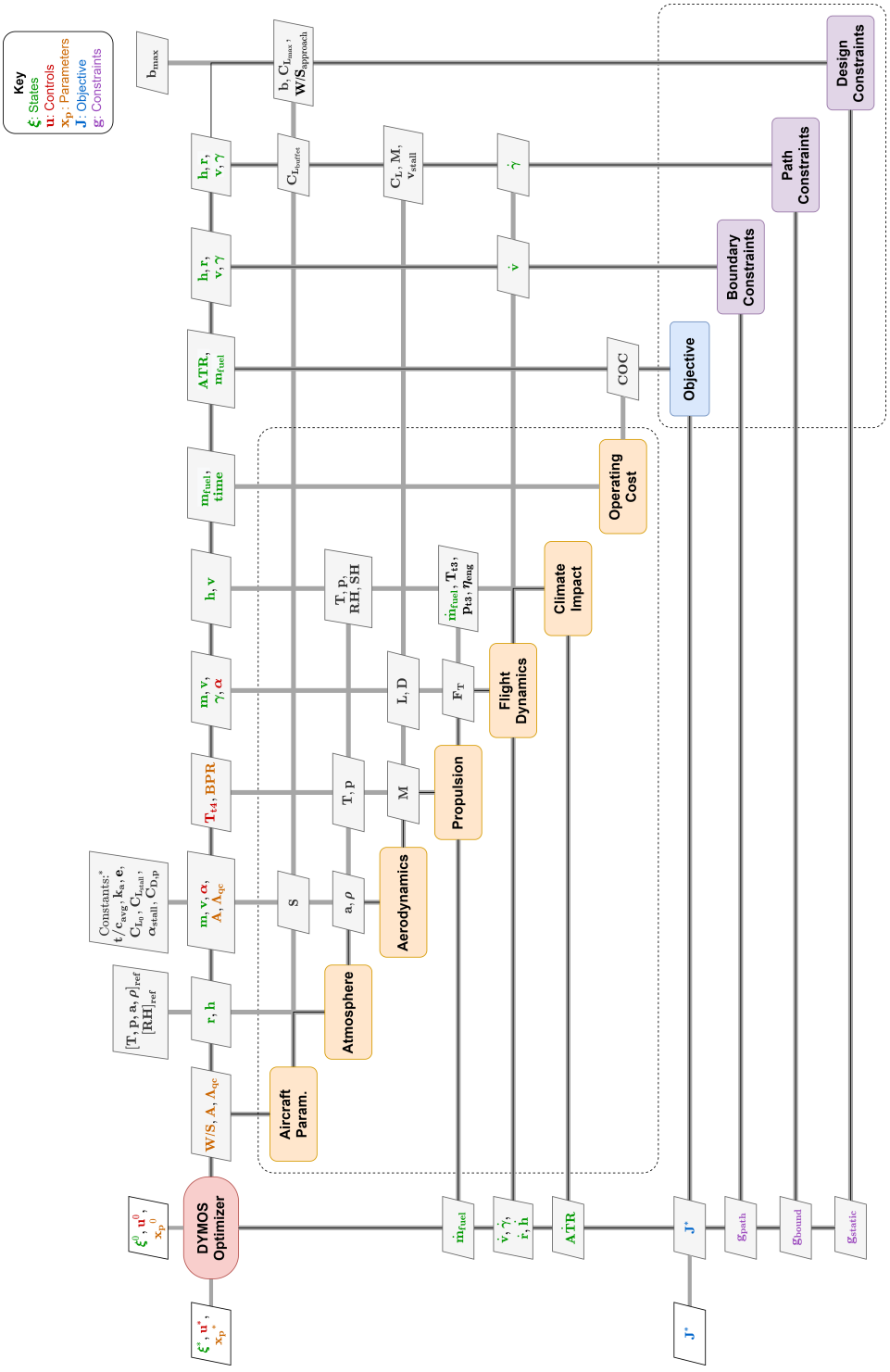

Figure A.1: Full Extended Design Structure Matrix

B

Climate Impact Response Functions

B.1. Atmospheric Perturbation Response Functions

For carbon dioxide, the response function given by [53] is:

$$G_{\chi_{CO_2}}(t) = \sum_{i=1}^{5} \alpha_i \cdot e^{-1/\tau_i} \tag{B.1}$$

Coefficients α_i and τ_i are given in table B.1.

Table B.1: Coefficients and Perturbation Lifetimes for CO_2 Response Function $G_{\chi_{CO_2}}$ [53].

i	1	2	3	4	5
α_i	0.067	0.1135	0.152	0.0970	0.041
τ_i	∞	313.8	79.8	18.8	1.7

The decay of methane and ozone are modelled by the response function $G_i(t)$, for $i = CH_4$, O_{3L}.

$$G_i(t) = A_i \cdot e^{-t/\tau_i} \tag{B.2}$$

A_i is taken from the RF/E_{ref_i} value in table B.2. A perturbation lifetime of 12 years is assumed.

B.2. Climate Efficacy and Radiative Forcing Sensitivity

For each species, the efficacy and radiative forcing sensitivity are given in table B.2.

Table B.2: Efficacy (f_i) and Radiative Forcing Sensitivity (RF/E_{ref_i}) of Climate Impacting Species.

Species	Efficacy f_i	Source f_i	RF/E_{ref_i}
CO_2	1.00	[55]	1.80×10^{-15} (W/m^2/kg)
CH_4	1.18	[55]	-5.16×10^{-15} (W/m^2/kg)
O_{3L}	1.37	[55]	-1.21×10^{-13} (W/m^2/kg)
O_{3S}	1.37	[55]	1.01×10^{-11} (W/m^2/kg)
H_2O	1.14	[55]	7.43×10^{-15} (W/m^2/kg)
SO_4	0.90	[56] Sec. 2.8.5.5	-1.00×10^{-10} (W/m^2/kg)
Soot	0.70	[56] Sec. 2.8.5.6	5.00×10^{-10} (W/m^2/kg)
Contrails	0.59	[55]	1.82×10^{-12} (W/m^2/km)

B.3. Altitude Dependency

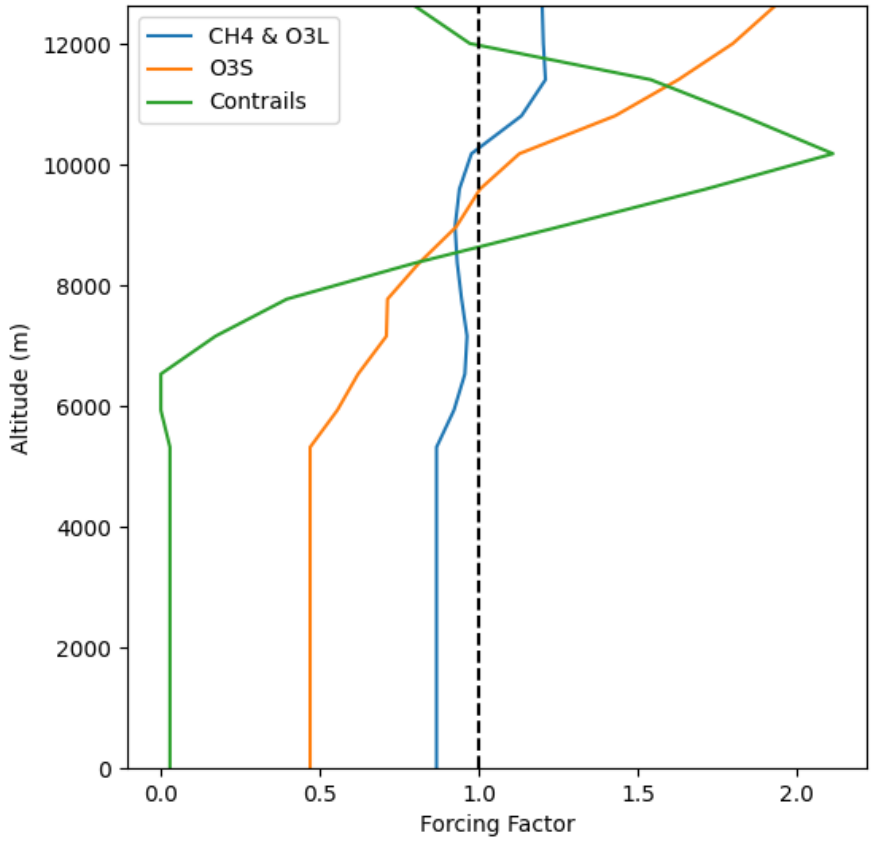

Figure B.1: Altitude Forcing Factors of Different Compounds [41].

C

Collocation Point Illustration

This appendix gives an illustration of how collocation points are chosen based on Legendre Polynomials of different order. The methods of *Legendre-Gauss* (LG), *Legendre-Gauss-Radau* (LGR) and *Legendre-Gauss-Lobatto* (LGL) are shown. For each method, collocation nodes are based on the roots of Legendre polynomials where the interval (-1, 1) corresponds to the discretised subinterval. For N collocation nodes and Legendre polynomials of N_{th}-degree as $P_N(\tau)$, the chosen nodes are:

- LG: Roots of $P_N(\tau)$
- LGR: Roots of $P_{N-1}(\tau)$ + $P_N(\tau)$
- LGL: Roots of $\dot{P}_{N-1}(\tau)$ including points -1 and 1

The Legendre polynomials and nodes are shown for fourth order LG, LGR and LGL methods in figures C.1, C.2 and C.3 respectively. Polynomial roots are shown as black dots, while added endpoints for LGL nodes are in red.

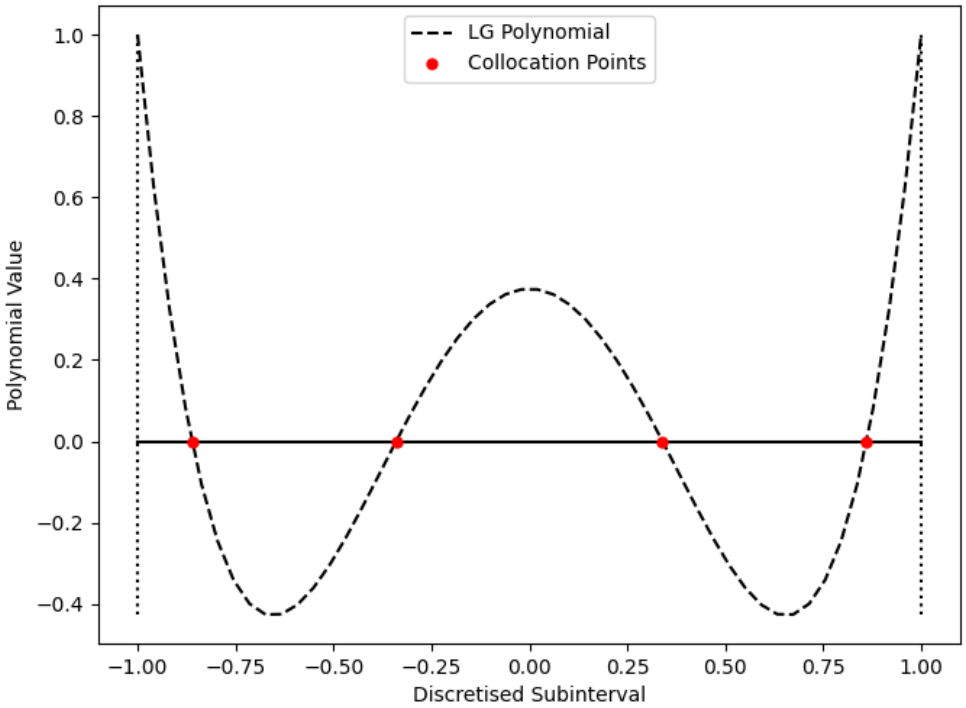

Figure C.1: Fourth Order Legendre-Gauss Collocation Points.

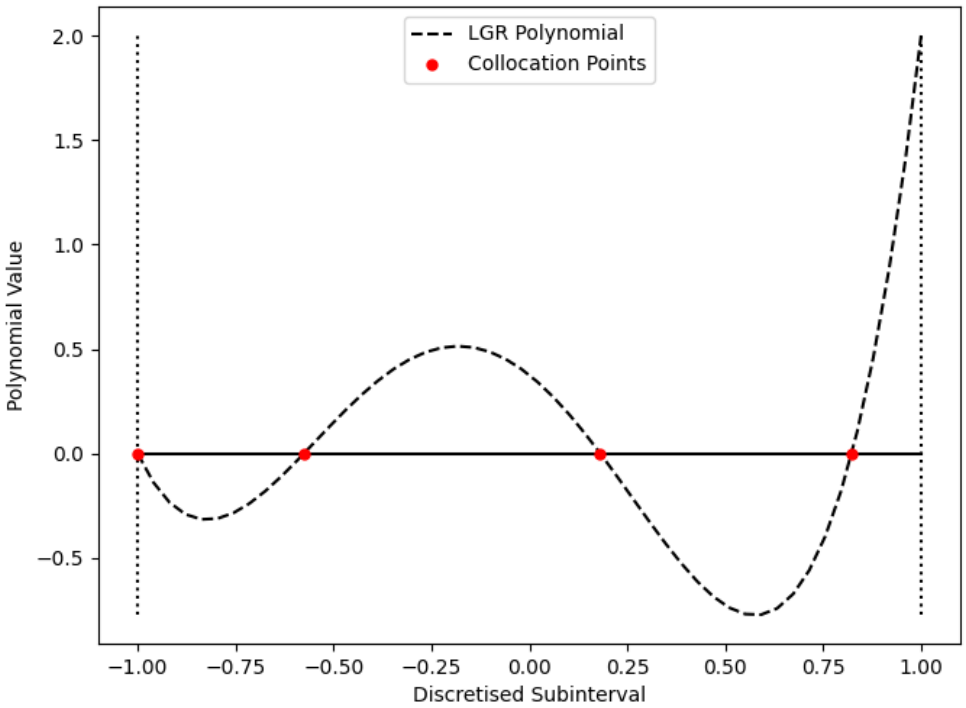

Figure C.2: Fourth Order Legendre-Gauss-Radau Collocation Points.

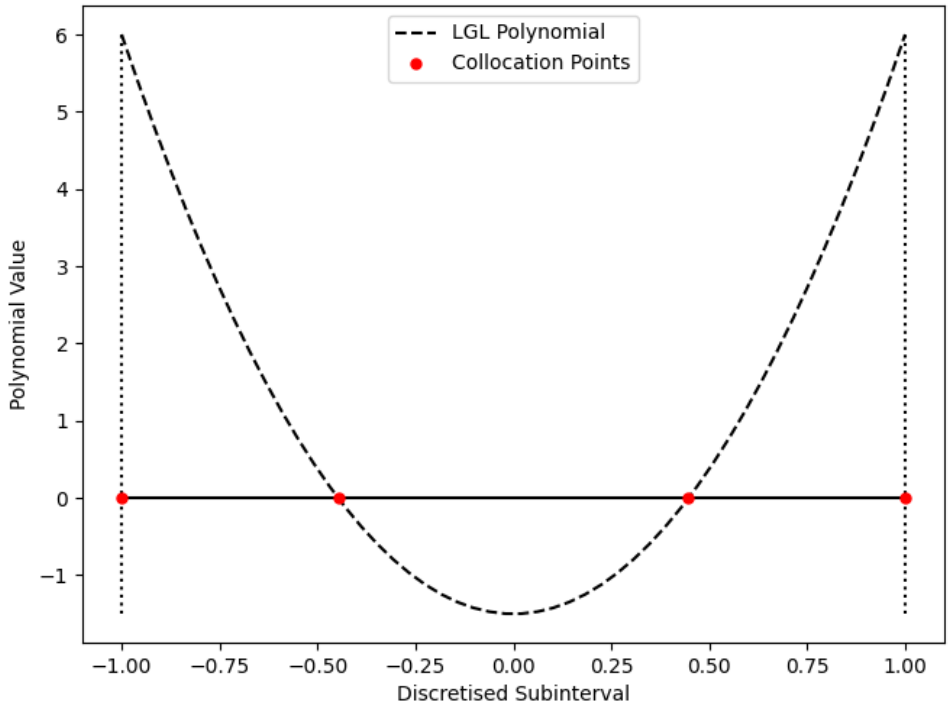

Figure C.3: Fourth Order Legendre-Gauss-Lobatto Collocation Points.

D

Propulsion Model Verification

An analytical surrogate propulsion model was developed to closely match the results of the model developed by Proesmans and Vos [1]. Overlaid plots of all outputs of the propulsion module are provided, comparing the surrogate model developed in this work with the 'full' model. The plots are based on the medium range baseline trajectory. Differences between the results are negligible. The only visible difference in these plots is in engine efficiency, which has a small impact on contrail formation properties.

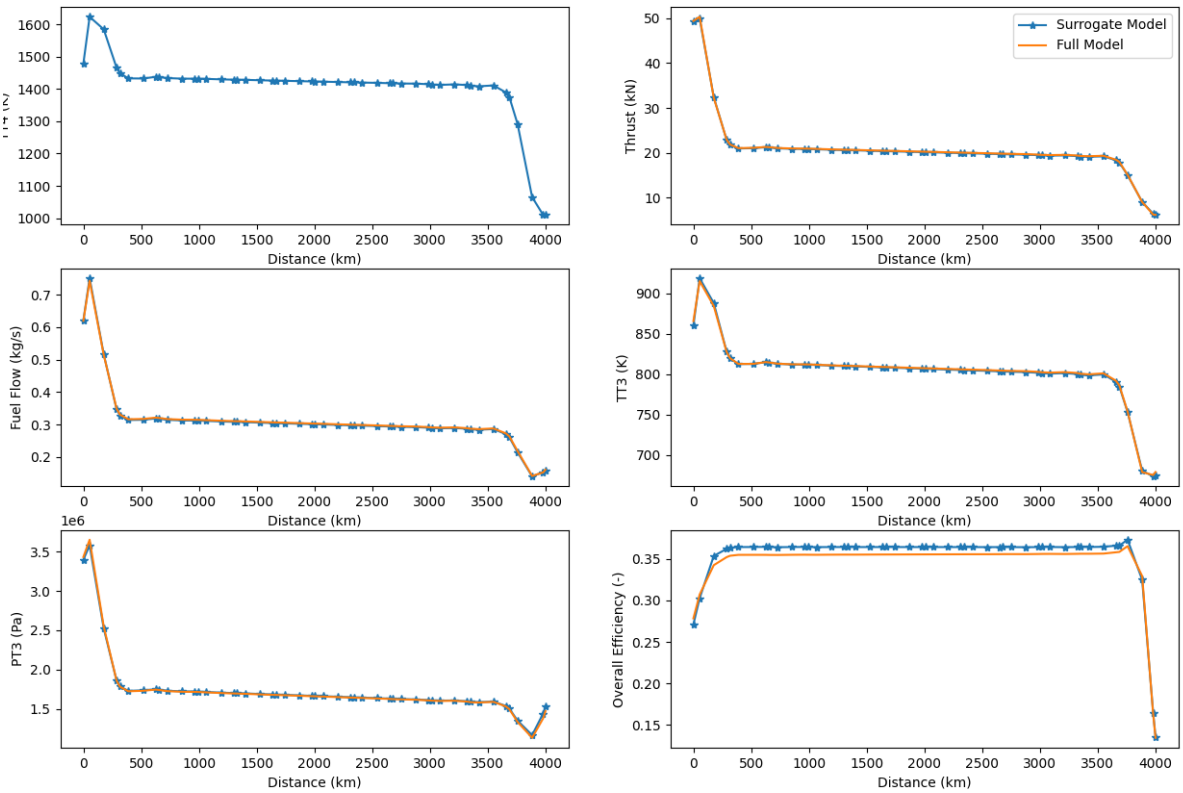

Figure D.1: Propulsion Verification Plots Based on the Reference Cost-Optimal Trajectory.

E

Contrail Persistence Criteria Variation

The binary nature of the contrail persistence criteria described in Section 3.4.2 is unrealistic and causes difficulty for the trajectory optimiser. To address this, each of the three criteria (Schmidt-Applemann Criterion (SAC), freezing below -38°C and ice-supersaturation regions (ISSRs)) are smoothed using a hyperbolic tangent function depending on the proximity to satisfaction of the criteria. The weighting is applied to the resulting contrail RF, so that a climate impact gradient is detectable by the optimiser. Figure E.1 shows the weighting variation due to the SAC, which depends on temperature, pressure and humidity. Assuming a standard atmosphere, the pressure and temperature are inferred from altitude. Figure E.2 shows the persistence weighting variation due to ice-supersaturation, which is determined from the atmospheric temperature and humidity.

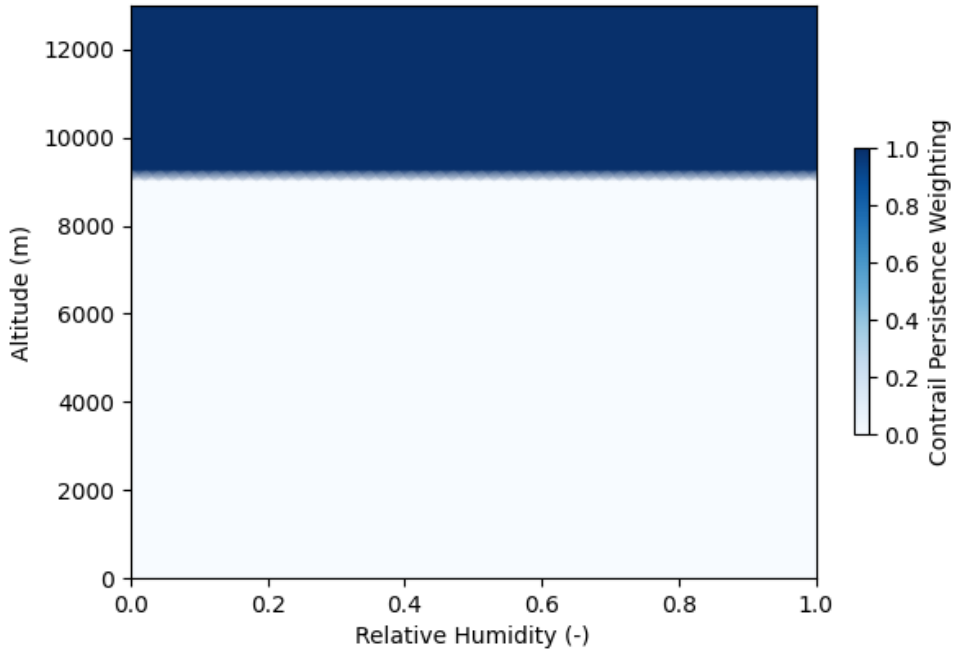

Figure E.1: Schmidt-Applemann Criterion Weighting Illustration.

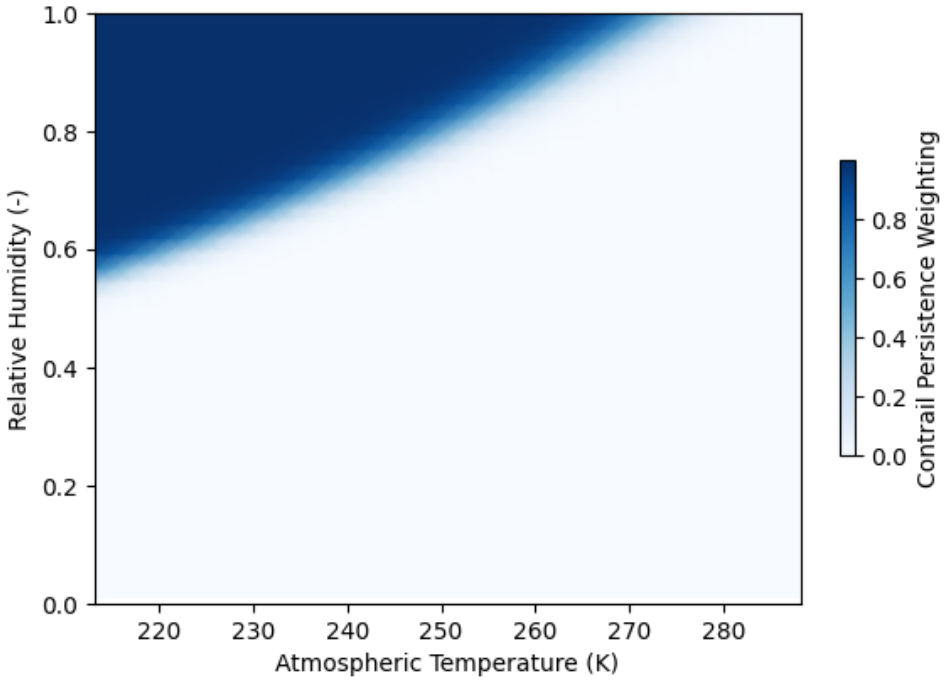

Figure E.2: Ice-Supersaturation Criterion Weighting Illustration.

F

Atmospheric Humidity Variation

As introduced in the case methodology (Section 3.5), atmospheric humidity varies with altitude and flight distance. Figure F.1 shows the reference data from Held [47] and the spline approximation used to create an atmosphere with smooth humidity variation, aiding the optimiser in gradient finding. Figure F.2 shows the horizontal variation in humidity to create the two cases studied in this work.

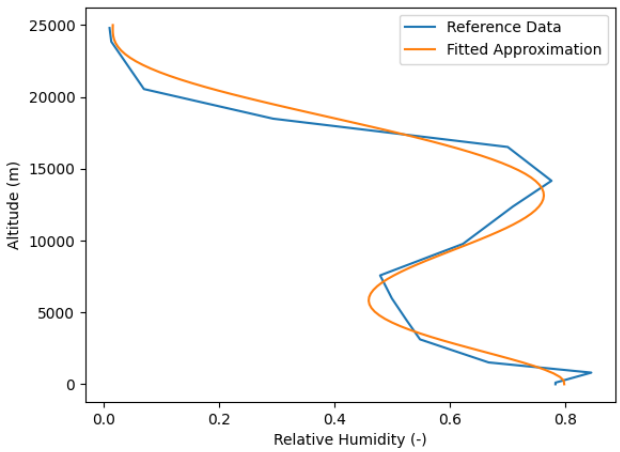

Figure F.1: Relative Humidity Variation with Altitude, Reference Data [47] and Fitted Spline Approximation.

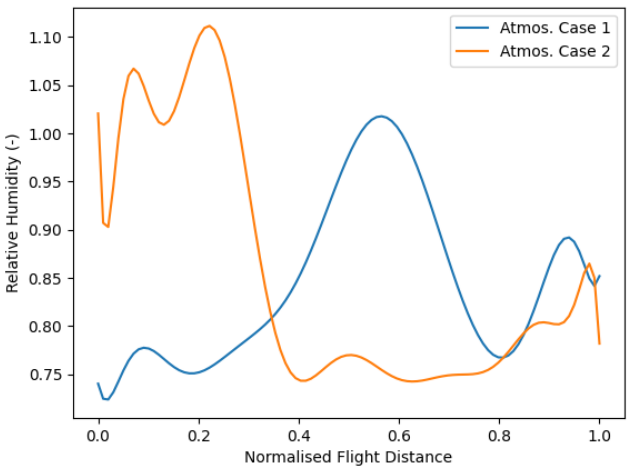

Figure F.2: Relative Humidity Variation for the Two Atmospheric Cases Studied.